

Erin A. Greguske<sup>1,2</sup>, Maria Carreres-Pons<sup>1</sup>, Blanca Cutillas<sup>3</sup>, Pere Boadas-Vaello<sup>4</sup>, Jordi Llorens<sup>1,2</sup>

**Calyx junction dismantlement and synaptic uncoupling precede hair cell extrusion in the vestibular sensory epithelium during sub-chronic 3,3'-iminodipropionitrile ototoxicity in the mouse**

<sup>1</sup> Departament de Ciències Fisiològiques, Institut de Neurociències, Universitat de Barcelona, Feixa Llarga s/n, 08907 L'Hospitalet de Llobregat, Catalunya, Spain

<sup>2</sup> Institut d'Investigació Biomèdica de Bellvitge, IDIBELL, 08907 L'Hospitalet de Llobregat, Catalunya, Spain.

<sup>3</sup> Departament d'Infermeria Fonamental i Medicoquirúrgica, Institut de Neurociències, Universitat de Barcelona, Feixa Llarga s/n, 08907 L'Hospitalet de Llobregat, Catalunya, Spain

<sup>4</sup> Research Group of Clinical Anatomy, Embryology and Neuroscience (NEOMA), Departament de Ciències Mèdiques, Facultat de Medicina, Universitat de Girona, 17003 Girona, Catalunya, Spain.

Corresponding autor: Prof. Jordi Llorens, Ph.D.; e-mail: [jllorens@ub.edu](mailto:jllorens@ub.edu); Ph: +34934024277

ORCID codes:

E.A.G.: 000-001-8536-7699.

M.C.-P.: 0000-0002-5379-898X

B.C.: 0000-0002-6088-0092

P.B.-V.: 0000-0001-8497-1207

J.L.: 0000-0002-3894-9401

Acknowledgements:

This study was supported by grants BFU2015-66109-R (MINECO/FEDER, EU), and 2017 SGR 621 (Agència de Gestió d'Ajuts Universitaris i de Recerca, Generalitat de Catalunya), and a Minor Research Grant from the Ménière's Society, UK. E.A.G. was supported by the Secretaria d'Universitats i Recerca del Departament d'Economia i Coneixement de la Generalitat de Catalunya (FI-DGR 2015 Program) and by the Ministerio de Educación, Cultura y Deporte de España (FPU 2015). The electron and confocal microscopy studies were performed at the Scientific and Technological Centers of the University of Barcelona (CCiT-UB). We thank Dr. Benjamín Torrejon-Escribano, Josep M. Rebled, Rosa Rivera and Adriana Martínez Gené for technical assistance and Natacha F. Kolar for animal care. We also thank Dr. Judit Homs and the students Meritxell Deulofeu, Sílvia Prades, Marc Bosch-Mola, Bertrán Álvarez-Pérez, Aina Espinosa, Judith Lloret, Júlia Valor, and Maria Capdevila for their contributions to the study.

## **ABSTRACT**

The cellular and molecular events that precede hair cell (HC) loss in the vestibular epithelium during chronic ototoxic exposure have not been widely studied. To select a study model, we compared the effects of sub-chronic exposure to different concentrations of 3,3'-iminodipropionitrile (IDPN) in the drinking water of two strains of mice and of both sexes. In subsequent experiments, male 129S1/SvImJ mice were exposed to 30 mM IDPN for 5 or 8 weeks; animals were euthanized at the end of the exposure or after a washout period of 13 weeks. In behavioral tests, IDPN mice showed progressive vestibular dysfunction followed by recovery during washout. In severely affected animals, light and electron microscopy observations of the vestibular epithelia revealed HC extrusion towards the endolymphatic cavity. Comparison of functional and ultrastructural data indicated that animals with fully reversible dysfunction did not have significant HC loss or stereociliary damage, but reversible dismantlement of the calyceal junctions that characterize the contact between type I HCs (HCI) and their calyx afferents. Immunofluorescent analysis revealed the loss of calyx junction proteins, caspr1 and tenascin-C, during exposure and their recovery during washout. Synaptic uncoupling was also recorded, with loss of pre-synaptic Ribeye and post-synaptic GluA2 puncta, and differential reversibility among the three different kinds of synaptic contacts existing in the epithelium. qRT-PCR analyses demonstrated that some of these changes are at least in part explained by gene expression modifications. We concluded that calyx junction dismantlement and synaptic uncoupling are early events in the mouse vestibular sensory epithelium during sub-chronic IDPN ototoxicity.

## **Keywords**

Ototoxicity. Vestibular system. Afferent terminals. Calyceal junctions. Ribbon synapses. 3,3'-Iminodipropionitrile.

## INTRODUCTION

The vestibular system in the inner ear detects head accelerations, including gravity and those resulting from linear and rotational movements of the head, to control gaze and body posture. Vestibular dysfunction causes disequilibrium and blurred vision, often accompanied by vertigo, dizziness and nausea, and may be a result of the loss of the mechanotransducer sensory hair cells (HCs) responsible for vestibular and auditory transduction. Several drugs and chemicals target the HCs and are thusly named ototoxic compounds. The main examples, and the more relevant ototoxic compounds pertaining to human health, are aminoglycoside antibiotics (Schacht et al., 2012). Other ototoxic chemicals are the antineoplastic agent cisplatin (Paken et al., 2016; Callejo et al., 2017) and several pollutants and industrial chemicals (Hodgkinson and Prasher, 2006). Many studies support the conclusions that these chemicals can trigger HC apoptosis (Li et al., 1995; Op de Beek, 2011; Schacht et al., 2012), and that the potential of HC regeneration is very limited (Llorens et al., 1993; Golub et al., 2012; Rubel et al., 2013; Taylor et al., 2015). This explains why the loss of function is commonly irreversible. However, there are varying degrees of functional recovery recorded in the vestibular function of patients after completion of the aminoglycoside treatment (Black et al., 2001, 2004). Although compensation mechanisms in the central nervous system may in part explain behavioral recovery (McCall and Yates, 2011), the observations reported by Black and colleagues (Black et al., 2001, 2004) suggest that toxic effects other than apoptotic cell loss can be associated with reversible or irreversible loss of function.

The exposure pattern and dose level are key modulators on the outcome of toxic exposures, as buffer and repair capacities combine with toxicokinetic and toxicodynamic factors to determine the final result. Therefore, the study of multiple models of exposure, including different dose levels, acute and chronic studies, and diverse species, are necessary for a comprehensive understanding of the toxicity of a compound or a class of compounds. In the case of ototoxicity, these studies have been limited by the relative resiliency of rats and mice to the ototoxic effects of aminoglycosides and cisplatin. Although many different animal models have been established to study these effects (Wu et al., 2001; Oesterle et al., 2008; Taylor et al., 2008; Murillo-Cuesta et al., 2010; Li et al., 2011; Breglio et al., 2017), there are remaining limitations in their flexibility to study the variety of toxicity responses that the inner ear can experience. This is revealed by the fact that, even after more than 50 years of research, new models often lead to the identification of new major phenomena, such as afferent terminal damage (Hirvonen et al., 2005; Ruan et al., 2014; Sultelmeier and Hoffman, 2017) or unique pharmacokinetic properties (Breglio et al., 2017).

Experimental studies have identified the ototoxic effects of several low molecular weight alkyl nitriles including: 3,3'-iminodipropionitrile (IDPN), racemic crotononitrile, allylnitrile, cis-crotononitrile, and cis-2-pentenenitrile (Llorens et al., 1993; Crofton et al., 1994; Llorens et al., 1998; Balbuena and Llorens, 2001, 2003; Gagnaire et al., 2001; Balbuena and Llorens, 2003; Boadas-Vaello et al., 2005; Soler-Martín et al., 2007; Saldaña-Ruíz et al., 2012 a,b). Except for cis-2-pentenenitrile (Saldaña-Ruíz et al., 2012a), human exposure is unlikely or very low (Tanii et al., 2004). Nevertheless, their use to study ototoxicity phenomena is supported by the many identified similarities between nitrile and aminoglycoside ototoxicity, and their greater

dependency of use in rodent models (Soler-Martín et al., 2007; Saldaña-Ruiz et al., 2013; Sedó-Cabezón et al., 2015).

Using IDPN as a model to study ototoxicity in the rat, we demonstrated that the main mode of HC loss in the vestibular sensory epithelium can shift from necrosis to apoptosis to HC extrusion as a function of the exposure model (acute, sub-acute, and sub-chronic, respectively) (Seoane et al., 2001b). In recent work, the same rat model has been used to identify afferent damage as an early and largely reversible event preceding HC extrusion during sub-chronic ototoxic exposure (Sedó-Cabezón et al., 2015).

In the present study, we have established an IDPN exposure model to study sub-chronic vestibular toxicity in the mouse. Using this model, we have determined the cellular events associated with slowly evolving vestibular dysfunction and recovery. In addition, we have identified several molecular events involved in these cellular and functional alterations.

## **MATERIALS AND METHODS**

### **Animals**

We used mice of the 129S1/SvImJ strain (129S1) from a locally established colony, which were descendants of previously purchased animals from Jackson Laboratory (Bar Harbor, ME, USA). We also used RjOrl:Swiss/CD-1 (Swiss) mice obtained from Janvier (Le-Genest-Saint-Isle, France) and acclimatized them for at least one week before experimentation. Animals were housed individually or up to 6 per cage in Macrolon cages (28×28× 15 cm) with wood shavings as bedding. The housing room was maintained at 22°C + 2°C with a 12:12 hour L:D cycle (0700 - 1900 h). Mice had unlimited access to standard diet pellets (TEKLAD 2014, Harlan Interfauna Ibérica, Sant Feliu de Codines, Spain) and to filtered and sterilized tap water. The animals were regularly weighed and evaluated for overall toxicity to limit suffering according to ethical criteria. For collection of the vestibular sensory epithelia and ganglia, the animals were anesthetized (400 mg/kg chloral hydrate, i.p.) and decapitated. The use and care of the animals was approved by the Ethics Committee on Animal Experimentation of the University of Barcelona and performed in accordance with Law 5/1995 and Act 214/1997 of the Generalitat de Catalunya, UE Directive 2010/63, and Law 6/2013 and Act 53/2013 of the Gobierno de España.

### **Groups and treatments**

In all experiments, IDPN (>98%, TCI Europe, Zwijndrecht, Belgium) was administered in the drinking water. Control animals received tap water only. Bottles were changed weekly and weighed to obtain a rough assessment of the dose ingested by the animals. During the exposure and recovery periods, mice were evaluated for vestibular dysfunction at several time points as shown in the results section.

Preliminary experiments were designed to identify the suitability of mice of different strains (129S1 and Swiss) and sex to study sub-chronic vestibular toxicity using the IDPN drinking water exposure model. They are described in Supplementary Methods. Final experiments used

a total of 97 adult male 129S1 mice exposed to 0 or 30 mM of IDPN. One IDPN animal died. Groups of animals were euthanized at 3 weeks (n=3 control and 6 treated), 5 weeks (n=7 and 17), or 8 weeks (n=9 and 22) of exposure. Additional control animals and animals exposed for 8 weeks (n=11 and 21, respectively) were euthanized after a washout period of 13 weeks. Many animals were used for more than one technique, and the number of animals for each result is indicated throughout the text and summarized in Supplementary Table 1.

### **Vestibular Dysfunction Ratings (VDRs)**

To assess the loss and recovery of vestibular dysfunction, we used a behavioral test battery that is sensitive and specific to vestibular function as reported previously for rats (Llorens et al., 1993; Llorens and Rodríguez-Farré, 1997; Boadas-Vaello et al., 2005; Sedó-Cabezón et al., 2015) and mice (Soler-Martín et al. 2007; Boadas-Vaello et al. 2007, 2009; Saldaña-Ruíz et al. 2012b, 2013). Briefly, animals were blindly evaluated on 6 items and rated on a scale of 0 to 4, with 4 being the score for maximal possible deviation from the behavior shown by normal, healthy animals. Animals could then receive a total VDR of 0 to 24 as the sum of the scores for the 6 rated items. The mice were first placed for one minute in a clean rat cage with no lid, which served as an open arena, and rated for circling (stereotyped circulatory ambulation), retropulsion (backward movement), and abnormal head movements (intermittent extreme backward extension of the neck). The mice were then rated for three anti-gravity reflexes: the tail-lift reflex, contact inhibition of the righting reflex, and the air-righting reflex. When lifted by the tail for the tail-lift reflex, vestibular-deficient mice bend or curl ventrally instead of extending the body and forelimbs towards the earth's center of gravity, which represents a landing response characteristic of healthy animals. For contact inhibition of the righting reflex, the animals were rotated into a supine position onto a horizontal surface, and a rigid, plastic board was lightly placed in contact with the soles of their feet. Vestibular-deficient mice lie on their back, with their feet up, and "walk" with respect to the ventral surface, while healthy mice quickly right themselves. For the air-righting reflex test, animals were flipped to a supine position in the air and dropped onto a foam cushion; vestibular deficient mice fail to right themselves in the air, while healthy mice do.

### **Ultrastructural assessment of the vestibular sensory epithelia**

The first dissected ear from each animal was used for ultrastructural studies while the second was used for immunohistochemistry. The right temporal bone was immediately immersed in ice-cold 2.5% glutaraldehyde in 0.1 M cacodylate buffer (pH 7.2) and the three cristae, the utricle, and the saccule were quickly dissected using a binocular microscope under a fume hood. After dissection, the vestibular epithelia were fixed for 1.5 h, rinsed with buffer, post-fixed for 1 h with 1% osmium tetroxide in the same buffer, rinsed again, and then placed in 70% ethanol and stored at 4°C until further processing. The samples were then dehydrated with increasing concentrations of ethanol up to 100%. For scanning electron microscopy (SEM), the anterior and posterior cristae, the utricle, and the saccule were dried in a Polaron 3000 critical point apparatus using liquid CO<sub>2</sub>, coated with carbon, and observed in a JEOL JSM-7001F field emission scanning electron microscope. For transmission electron microscopy (TEM), the lateral crista was embedded in Spurr resin. Semithin sections (1 µm) were stained with toluidine blue and observed in a light microscope in order to select specific regions for

TEM studies. Ultrathin sections were stained with uranyl acetate and lead citrate and examined in a JEOL 1010 electron microscope.

For SEM studies, each vestibular epithelium was assigned a SEM Pathology Score according to a scale of 0 to 5 as follows: 0 = absent pathology; 1 = presence of membrane blebs behind the stereociliary bundles; 2 = presence of a small proportion (<5% of the population) of overtly damaged stereocilia bundles, extruding, or missing HCs; 3 = significant presence (5-40 %) of overtly damaged stereocilia bundles, extruding, or missing HCs; 4 = extensive presence (40 – 80%) of overtly damaged stereocilia bundles, extruding, or missing HCs; 5 = most HCs (>80% of the population) are missing, extruding, or showing fused stereociliary bundles.

For TEM studies, the distance between the centers of adjacent membranes at the contact between type I HCs (HCI) and the calyx afferent was measured on TEM images (Sousa et al., 2009) using the Imaris software (Bitplane, Zurich, Switzerland). Images were obtained from transverse sections, perpendicular to the surface of the epithelium, of the lateral cristae at approximately 100-150  $\mu\text{m}$  from its longitudinal edge. To compare control animals with animals exposed to IDPN for 8 weeks and washout animals, we obtained data from 3 animals per group. For each animal, 12-19 unique HCIs, as sequentially identified in the TEM were analyzed. The localization of the cells within the epithelium varied in a pseudo-random distribution generated by the bars of the grids on which the tissue sections were mounted. For each HCI, we measured the distances at 20-25 points regularly distributed throughout the cell's basolateral membrane, from the basal end to the level of the upper end of the nucleus, where the calyceal junction is located in normal tissues (Sousa et al., 2009; Lysakowski et al., 2011; Sedó-Cabezón et al., 2015). For each point (total of 3,574 measurements), it was annotated whether the electrodense material characterizing the calyceal junction was present or absent.

### **Immunohistochemistry**

We used the mouse monoclonal anti-Caspr1 (clon K65/35; used at 1:400 dilution) antibody from the UC Davis / NIH NeuroMab Facility. Other mouse monoclonal antibodies used were the anti-GluA2 (clon 6C4, Millipore; 1:100) and anti-Ribeye/CtBP2 (clon 16/CtBP2, BD Transduction Labs, 1:100). As commercially available polyclonal antibodies, we used the rabbit anti-calretinin (7699/3H, Swant; 1:500), anti-myosin VIIa (25-6790, Proteus Biosciences; 1:400), and anti-tenascin (AB19013, Millipore; 1:200), and goat anti Na<sup>+</sup>/K<sup>+</sup>-ATPase  $\alpha$ 3 (SC16052, Santa Cruz, 1:300). To label nuclei, DRAQ5 was purchased from Abcam and was used in some cases (1:1000). The primary antibodies were revealed by secondary antibodies conjugated with Alexa Fluor -488, -555, and -647 fluorochromes. We used anti-mouse IgGs (A21202, A21425, A31571), anti-rabbit IgGs (A21206, A31572, A31573), anti-goat IgG (A21432), and specific anti-mouse IgG1 and IgG2a isotypes (A21121, A21131, A21127, A21240, A21137, A21241) from Invitrogen / Thermo Fisher. The specificity of the primary antibodies used to obtain the data in the present article has been well characterized (Supplementary Table 2). We performed controls omitting the primary antibody and found that non-specific staining was restricted to blood vessels for anti-mouse secondary antibodies. Conclusions and quantitative data presented here were derived from immunofluorescent images offering no doubt of the specificity of the label.

The dissected vestibular epithelia were fixed for 1 h at room temperature in 4 % paraformaldehyde in phosphate buffered saline (PBS) with 15% saturated picric acid. The specimens were then rinsed in PBS and stored at -20°C in a cryoprotective solution (34.5% glycerol, 30% ethylene glycol, 20% PBS, 15.5% distilled water). Whole vestibular epithelia were used for immunolabeling. Equal numbers of specimens from each experimental group were processed in parallel to equal batch-to-batch differences in label. Epithelia were permeabilized and blocked in 4% Triton-X-100 and 20% donkey serum in PBS for 90 min at room temperature. They were then incubated with the mixed primary antibodies in 0.1% Triton-X-100 and 1% donkey serum in PBS for 48 h at 4°C, followed by incubation with the secondary antibodies in 0.1% Triton-X-100 in PBS overnight at 4°C, or for 2 h at room temperature. The samples were thoroughly rinsed with PBS following each incubation. When used, DRAQ5 was applied to the PBS for 15 min between the final washes. The samples were gently rocked during the incubations and washes. Once stained, the epithelia were embedded in 0.49% gelatin, 30% bovine serum albumin, and 20% sucrose in PBS overnight at 4 °C. Then, a block was formed with the same media solidified with 9% glutaraldehyde, with one epithelium oriented on its surface, and a second block was formed over top of it. This layered block, with one specimen situated in between the two halves, was used to section the sample at 40 µm in a Leica VT100M vibrating microtome (Leica Microsystems CMS GmbH, Mannheim, Germany). Finally, sections were mounted in Mowiol medium.

### **Confocal microscopy observation and analysis**

A Leica TCS-SL confocal microscope was used for the assessment of the vestibular epithelia after immunofluorescent labeling. All sections from any given specimen were examined. Quantitative data were obtained from optimally oriented sections from the central parts of the neuroepithelium. These sections are most favorable to study all three possible HC-afferent arrangements: HCI-calyx-only units (identified by calretinin labeling of the calyx afferent), HCII-bouton units (identified by shape and calretinin labeling of the HC), and HCI-dimorphic units (calyces with no calretinin label). Images were acquired with the 63X objective at zoom level 2. Identical acquisition settings were used when obtaining images from each different treatment group. For quantitative analysis, 50-image Z stacks of 0.5 µm thick optical sections were obtained, spanning a total of 25 µm, and these series were combined into 5 serial snapshots by projecting 10 consecutive images. To study calyceal junctions, the complete stacks from 2 different tissue sections were counted for each of 6 control mice, 3 mice treated with IDPN for 8 weeks, and 5 mice after the washout period. From each animal, the total number of calyces with distinct Caspr1 or Tenascin-C immunoreactivities, and their colocalizations were obtained. To study synaptic elements, the number of Ribeye/CtBP2 puncta, GluA2 puncta, and the Ribeye-GluA2 colocalization were determined in synapses from three different HC-afferent arrangements. The number of puncta per cell was obtained from 169 cells from 9 control animals, 147 cells from 5 IDPN 8-week animals, and 188 cells from 6 washout animals. The number of cells counted per unit type and treatment group varied between 25 and 74.

### **qRT-PCR**

Ears were dissected in ice-cold PBS and the two vestibular ganglia or all vestibular epithelia (six cristae and two utricles) per animal were pooled together. Total RNA was extracted using the

Qiagen RNeasy mini kit and protocol. Samples were quantified with an Agilent Bioanalyzer 2100 (Agilent Technologies, Santa Clara, CA, USA). Equal quantities of total RNA were reverse transcribed using a High-Capacity cDNA Reverse Transcription Kit (Applied Biosystems, Alcobendas, Spain). Equal amounts of cDNA (15ng) were used for RT-PCR analysis. Actin beta (Actb) was used as the internal control gene. The RT-PCR was performed with a SensiFAST Probe Hi-ROX kit (Bioline, Barcelona, Spain) in duplicate with the following Taqman assays (Life Technologies, Alcobendas, Spain): Mm00607939\_s1 (Actb), Mm00495662\_m1 (Tnc), Mm00515572\_m1 (Ctbp2), Mm 00489702\_m1 (Cntnap1), and Mm00442828\_m1 (Gria2). Reaction mixtures (10  $\mu$ l) were first incubated at 50°C for 2 min and then at 95°C for another 10 min, followed by 40 cycles (95°C for 15 s and then 60°C for 1 min) of PCR. Real-time fluorescence was detected using a 7900 HT Real-Time PCR System (Applied Biosystems). Threshold cycles (Ct) were analyzed using Expression Suite software, and a relative quantification method ( $\Delta\Delta$ Ct) was used to calculate target gene expression according to the Guide to Performing Relative Quantitation of Gene Expression Using Real-Time Quantitative PCR (Applied Biosystems).

### **Data analysis**

Data are presented as mean  $\pm$  SE, except where indicated otherwise. Body weight and vestibular dysfunction data were analyzed with repeated-measures MANOVA (Wilks' criterion), or repeated-measures ANOVA (Greenhouse-Geiser correction), depending on the number of degrees of freedom available. Day was the within-subject factor. Day-by-day analysis was performed after significant day-by-treatment interactions were recorded. Other data were analyzed by appropriate ANOVA designs and Duncan's post-hoc test, or by Student's t-test. The IBM SPSS Statistics 20 program package was used.

## **RESULTS**

### **Preliminary experiments to establish a mouse model of sub-chronic vestibular toxicity**

In the preliminary experiments, mice of different strains and sexes exposed to IDPN via drinking water showed different concentration-response relationships for vestibular and systemic toxicities. In these experiments (Supplementary Figure 1), male 129S1 mice exposed to 30 mM IDPN showed progressive vestibular dysfunction with limited systemic toxicity and was consequently determined to be the most appropriate model to investigate chronic vestibular toxicity. Other combinations of strain, sex and IDPN concentration resulted in insufficient vestibular effects, excessive variability among individual animals and/or excessive systemic toxicity. Therefore, this strain, sex and concentration were selected for further study.

### **Effects of sub-chronic IDPN on body weight**

Male 129S1 mice exposed to 30 mM IDPN showed a slight reduction, followed by a slight increase, in body weight, which differed from the continuous gain in body weight shown by control animals (Figure 1A). The maximal decrease was recorded at 2 weeks of exposure, when IDPN animals had 97% of their initial weight, compared to 103.8% in control mice. At the end of the 8-week exposure period, control animals and treated animals showed 109.8% and

101%, respectively, of initial mean values. After the end of the exposure period, IDPN animals regained an increase in weight, but did not show a rebound effect; they showed 109.2% of their initial body weight at week 20, compared to 125.6% in control animals. The body weight data were analyzed in two separate MANOVA tests. Data from the exposure period (weeks 0 to 8) resulted in significant day ( $F[8,55]=7.66$ ,  $p<0.001$ ), treatment ( $F[1,62]=9.45$ ,  $p=0.003$ ), and day by treatment interaction ( $F[8,55]=5.55$ ,  $p<0.001$ ) effects. Data from the washout period (weeks 9 to 20) resulted in significant day ( $F[7,18]=8.64$ ,  $p<0.001$ ) and treatment ( $F[1,24]=9.72$ ,  $p=0.005$ ) effects, but the day by treatment interaction was not significant ( $F[7,18]=0.94$ ,  $p=0.504$ ), indicating a similar evolution of the body weight in both groups across time during this period.

### **Effects of sub-chronic IDPN on vestibular function**

Mice exposed to IDPN for up to 8 weeks showed a loss of vestibular function that progressed over time. The maximal VDRs (Fig. 1B) were observed at week 8 of the exposure ( $8.5\pm 0.9$ ,  $X\pm SE$ ) and were well below the maximal possible VDR of 24. Termination of the IDPN exposure resulted in a decrease in VDRs to near-control values, although a small but significant group difference was still found after 12 weeks of washout. VDR data were analyzed in two separate MANOVA tests. Data from the exposure period (weeks 0 to 8) resulted in significant day ( $F[7,32]=21.1$ ,  $p<0.001$ ), treatment ( $F[1,38]=59.3$ ,  $p<0.001$ ), and day by treatment interaction ( $F[7,32]=16.4$ ,  $p<0.001$ ) effects. Data from the washout period (weeks 9 to 20) resulted in significant day ( $F[8,11]=3.97$ ,  $p=0.019$ ), treatment ( $F[1,18]=25.2$ ,  $p<0.001$ ), and day by treatment interaction ( $F[8,11]=3.33$ ,  $p=0.034$ ) effects, supporting the conclusion that significant recovery in vestibular function occurred after termination of the exposure.

### **SEM analysis of stereociliary damage and HC loss following sub-chronic IDPN exposure**

SEM observation of the vestibular sensory epithelia revealed the apical surfaces of the HCs, characterized by the stereociliary bundles protruding from the cell's cuticular plate, and of the supporting cells, characterized by their abundant microvilli. In most control specimens (Fig. 2A), the appearance and density of the stereociliary bundles matched the literature descriptions for epithelia from healthy adult rats and mice (Dechesne et al., 1986; Soler-Martín et al., 2007; Saldaña-Ruiz et al., 2013), and were given a pathology score of 0. Nevertheless, some control samples attained SEM Pathology Scores of 1 or 2, as they displayed blebs or stereociliary fusion in a small number of HCs, respectively. Blebs are minor pathological alterations often recorded in control vestibular epithelia, likely due to hypoxia during dissection, as they are known to be formed within a few minutes of HC stress (Shi et al., 2005; Goodyear et al., 2008).

The effect of drinking 30 mM of IDPN on surface morphology varied according to the time-point and the vestibular epithelia considered. In all cases, saccules from IDPN animals presented a control-like morphology. In contrast, IDPN had an observable impact on the utricles, as illustrated in Fig. 2. At 5 weeks of IDPN exposure, when the animals were starting to show the very initial loss of vestibular function, the surface morphology was similar to that of control animals. The same morphological features were recorded in four animals exposed for 8 weeks and showing low (3 to 6) VDRs (Fig. 2B). In contrast, three mice that showed VDRs of 10 to 11 at 8 weeks of exposure displayed some loss of cells, stereocilia fusion and HC extrusion in

the peri-striolar area. These were given SEM Pathology Scores of 2 to 3 (Fig. 2C-E). The appearance of coalescence, the fusion of stereocilia into a single identity, has been described in many models of HC damage, including sub-chronic IDPN in rats (Seoane et al., 2001b), and likely represents a step in HC extrusion (Seoane et al., 2001a, b; Sedó-Cabezón et al., 2015). The worst-case example (Fig. 2F-G; SEM Pathology Score of 4) corresponded to a mouse with a VDR of 18. Washout animals examined at 13 weeks after the end of the 8-week exposure period displayed intact morphology (SEM Pathology Score of 0, Fig. 2H) or limited pathological alterations (SEM Pathology Scores of 1 to 2, Figure 2I-J).

Fig. 2K summarizes the relationship between the vestibular dysfunction of the animals at the end of the exposure period and the SEM Pathology Scores. The data reveal that a significant loss of function occurs in association with Pathology Scores of 0 to 2, that is, before a significant proportion of HCs are severely damaged or lost (scores of 3 to 5). In Fig. 2L, the relationship between the VDRs at both the end of the exposure period and after recovery, and the SEM Pathology Scores is shown. The data indicate that the initial dysfunction revealed by low to moderate VDRs (4 to 15) is fully or largely reversible when associated with low Pathology Scores (0 to 2).

The effect of the treatment on the crista was similar or larger than in the utricles, resulting in the same or same+1 pathology scores (Supplementary Fig. 2).

#### **Light microscopy and TEM analysis of calyceal junction loss, stereociliary fusion, and HC extrusion following sub-chronic IDPN exposure**

Transverse sections of the lateral crista examined by light microscopy and TEM displayed morphological features matching normative descriptions of vestibular cristae from adult healthy mice (Fig. 3A-C, Desai et al., 2005). The vestibular epithelium contains two types of HCs that differ in shape and afferent innervation. Type I HCs (HCI) have an amphora-like shape and are encased by a unique afferent, named a calyx, that covers the entire basolateral membrane of the cell (Fig. 3A). Type II HCs have a more cylindrical shape and are contacted by standard synaptic bouton contacts (Fig. 3B). The epithelium also contains supporting cells that separate the HCs, are in contact with the basal membrane, and have their nuclei at the low end of the epithelium (Fig. 3A-C). The lower half of the contact between the HCI and the calyx afferent shows the calyceal junction, an adhesion specialization characterized by the accumulation of an electron density on the plasma membrane on both sides with a constant spacing between them (Fig. 3C, J).

In mice exposed to IDPN for 5 weeks, the epithelium had an overall control-like appearance. However, some of the HCI-calyx afferent contacts were altered; the alteration consisted of partial to complete absence of the calyceal junction and fragmentation of the afferent (Fig. 3D). These morphologies are not recorded in healthy epithelia. After 8 weeks of exposure to IDPN, morphological abnormalities were diverse in different animals. Mice in this group showing low (3 to 6) VDRs displayed similar morphology to that described for 5-week animals, with occasional loss of the calyceal junction (Fig. 3E) and calyx fragmentation. In the three animals with VDRs in the 10-11 range, the dismantlement of the calyceal junctions was widespread, and some extruding HCs were recorded in one of them (Fig. 3F). In semithin sections from the crista of the worst-case example (VDR=18), we recorded widespread loss of

HCs, the presence of completely extruded HCs in the endolymphatic cavity, and extruding HCs (Fig. 3G). Under TEM observation, dismantlement of the calyceal junctions and calyceal fragmentation was extensive. Some of the extruding HCs showed signs of degeneration (Fig. 3H), while others kept an apparently undamaged cytoplasm and nucleus, as illustrated in Fig. 3F. The ultrastructural morphology of cristae from animals examined after the washout (n=3) resembled that of control animals, with clearly visible calyceal junctions (Fig. 3I).

The dismantlement of the calyceal junctions was assessed by measuring membrane-to-membrane distances in the HCl-calyx afferent contacts, as illustrated in Fig. 3J-K. These distances are smaller and more regular in places where the calyceal junction is present according to the presence of an electronic density in both membranes. The mean distance measured in these places was only slightly larger in 8-week mice ( $29.5 \pm 9.1$  nm, X+SD) compared to the mean in control mice ( $26.8 \pm 4.9$  nm) ( $p < 0.05$ , Duncan's test after significant ANOVA,  $F [2, 2274] = 41.5$ ,  $p < 0.001$ ). The mean distance in washout animals ( $26.5 \pm 5.0$  nm) did not differ from that in controls ( $p > 0.05$ ). These values agree with previous literature data ( $28 \pm 4$  nm, Sousa et al. 2009). However, the proportion of places that were identified as presenting an intact calyceal junction was lower in 8-week animals (40%) than in control (71%) and washout (76%) mice. Consequently, when the distances were compared including all points, it was found that IDPN animals had a 60% increase in mean membrane-to-membrane distance compared to controls ( $p < 0.05$ ), and that this was reduced to a 17% increase after washout (Fig. 3L). ANOVA results for the data in Fig. 3L are  $F[2, 3571]=104.7$ ,  $p < 0.001$ .

#### **Molecular analysis of calyceal junction dismantlement and synaptic uncoupling following sub-chronic IDPN exposure**

As a first step towards the identification of the molecular events taking place during early chronic vestibular toxicity, we used immunofluorescent analysis to study the alterations in the expression of proteins that characterize the calyceal junction or the synapses between the HCs and the post-synaptic afferents. All the animals used in this part of the study showed moderate levels of vestibular dysfunction (VDRs between 5 and 13 at 8 weeks of exposure). According to the SEM and TEM results above, these animals were showing significant to extensive loss of calyceal junctions, but very limited HC extrusion or loss. All the animals studied at washout had VDRs ranging from 6 to 12 at the end of the 8-week exposure period, which regressed to VDRs within the control range (0 to 2) after washout.

In the first series of immunofluorescent analyses, the calyceal junction was examined. Cristae were immunolabelled with antibodies against the Na<sup>+</sup>/K<sup>+</sup> ATPase alpha-3 subunit (NKAA3), which labels the plasma membrane of afferent terminals (Schuth et al., 2014; Fig. 4A a, d), against Caspr1, which localizes at the neuronal membrane of the calyceal junction (Sousa et al., 2009, Fig. 4A b, d), and against Tenascin-C, which localizes in the extracellular matrix of the same area (Lysakowski et al., 2011, Fig. 4A c, d). In mice exposed to 30 mM IDPN for 8 weeks (Fig. 4A e-h), we observed a dramatic reduction in Caspr1 and Tenascin-C immunoreactivity. The expression of these proteins in the calyceal junction area was reestablished in the washout mice (Fig. 4A i-l). For the quantitative analysis, we counted the number of visible calyceal regions demarcated by each calyceal protein, and their colocalization, from two different tissue sections per mouse. The data (Fig. 4B) clearly demonstrated the loss in Caspr1 and

Tenascin-C expression in the calyceal junction areas following IDPN exposure. ANOVA comparisons indicated significant group differences in Caspr1 ( $F[2,11]=175.1$ ,  $p<0.001$ ), Tenascin-C ( $F[2,11]=15.0$ ,  $p=0.001$ ), and their colocalization ( $F[2,11]=15.6$ ,  $p=0.001$ ). Recovery was complete for Tenascin-C and incomplete for Caspr1. These alterations in Caspr1 and Tenascin-C positive areas were not a secondary consequence of a loss and regrowth of the calyceal afferents, as these were still in place in the IDPN 8-week animals (Fig. 4A e, h), albeit some alterations of the calyceal shapes were also evident.

We also examined the integrity of the HC-afferent synapses at the immunoreactivity level. Cristae were immunolabeled with antibodies against Ribeye/CtBP2, to label pre-synaptic puncta in the HCs, against GluA2, to label post-synaptic puncta in the afferent terminals, and against calretinin (Fig. 5). The calretinin label allows for the identification of the three types of HC-afferent units: HCI-calyx units with calretinin-positive calyces from calyx-only afferents, HCI-calyx units with calretinin-negative calyces from dimorphic afferents, and HCII units identified by their shape and calretinin immunoreactivity (Desai et al., 2005). The overall morphology of cristae was drawn by the nuclear label of the CtBP2 protein, which is encoded by the same gene as Ribeye and recognized by the anti-Ribeye/CtBP2 antibody (Fig 5A a, e, i). Observations indicated a loss of synaptic elements in IDPN 8-wk animals (Fig. 5A e-h, n), followed by a recovery after washout (Fig. 5A i-l). For quantitative analysis, pre- and post-synaptic puncta were examined at high magnification as illustrated in Fig. 5A o-p. The data obtained (Fig. 5B) demonstrated group differences in the number of Ribeye puncta per cell in either HCI/calyx-only ( $F[2, 115]=14.73$ ,  $p<0.001$ ), HCI/dimorphic ( $F[2, 202]=15.83$ ,  $p<0.001$ ), and HCII ( $F[2, 179]=12.74$ ,  $p<0.001$ ) units. There was a reduction in Ribeye puncta in all three unit types after IDPN exposure; this was followed by a complete recovery in dimorphic units, but only partial recoveries in calyx-only and HCII units. The behavior of GluA2 puncta and of the Ribeye/GluA2 colocalization was similar, although with a smaller statistical robustness. Significant ANOVA results were obtained for GluA2 in HCII ( $F[2, 179]=3.60$ ,  $p=0.029$ ), colocalization in HCII ( $F[2, 179]=4.42$ ,  $p=0.013$ ), and colocalization in dimorphic units ( $F[2, 202]=3.99$ ,  $p=0.020$ ), while GluA2 results in both calyx-only and dimorphic units showed marginal significance ( $0.05<p<0.1$ ). In all cases, mean IDPN values were smaller than mean control values, and significant recovery was recorded in the washout animals. As with Ribeye, recovery was complete for colocalization numbers in dimorphic units, while recovery was incomplete in GluA2 and colocalization means in HCII units.

A preliminary evaluation of the role of gene expression in calyceal junction dismantlement and synaptic uncoupling was done by qRT-PCR analysis of the vestibular epithelium and ganglion (Fig. 6). In the vestibular epithelium, there was a reduction in the expression of Tnc, the gene encoding the extracellular matrix protein Tenascin-C, after IDPN exposure, which was recovered after washout ( $F[2,18]=5.7$ ,  $p=0.012$ ). In the vestibular ganglion, Tnc was expressed at approximately 20-fold lower levels, and this expression was not reduced following IDPN exposure (data not shown). In the ganglion, the mRNA expression of the adhesion molecule Caspr1 (Cntnap1 gene) was not modified. The Ctbp2 gene, encoding the pre-synaptic protein Ribeye, showed reduced expression after IDPN exposure that persisted after washout ( $F[2, 18]=9.68$ ,  $p=0.001$ ) in the vestibular epithelium. In the post-synaptic ganglion, the Gria2 gene, encoding the GluA2 receptor, showed an increase in expression after washout, while an

apparent reduction in expression after IDPN exposure did not reach statistical significance by post-hoc analysis after significant ANOVA results ( $F[2,22]=4.38$ ,  $p=0.025$ ).

## DISCUSSION

It is well established that several chemicals can induce HC loss in the vestibular epithelium, and that this results in irreversible dysfunction in mammals (Schacht et al., 2012). However, significant functional recovery is often recorded in clinical practice (Black et al., 2001, 2004), and the cellular and molecular basis of this loss and recovery of vestibular function remain mostly unexplored. Understanding these processes should allow us to better predict the reversibility of induced functional loss, to identify candidate targets for pharmacological blockade to stop the transition from reversible to irreversible damage, or for ameliorating or accelerating the recovery processes. Traditionally, most studies on ototoxicity have focused on models causing rapid HC degeneration (e.g., Taylor et al., 2008; Li et al., 2011), but the need to understand other consequences of ototoxicity is starting to be appreciated (Hirvonen et al., 2005; Sedó-Cabezón et al., 2014, 2015; Gaboyard-Niay et al., 2016; Sultemeier and Hoffman, 2017).

We have previously established a rat model of sub-chronic ototoxicity (Llorens and Rodríguez-Farré, 1997; Seoane et al., 2001a, 2001b) that shows a reversibility that varies according to the length of the exposure (Sedó-Cabezón et al., 2015). Using the same toxic compound, IDPN, we have now established a mouse model, and used it to identify cellular and molecular steps involved in reversible and irreversible loss of vestibular function. We tested two strains of mice and both sexes at different exposure concentrations of IDPN in the drinking water, and selected one single combination for further studies: male 129S1 mice exposed to 30 mM of IDPN. In this model, animals showed a progressive decline in vestibular function with little systemic toxicity, limited to a halting of body weight gain. Other combinations of strain, sex, and concentration showed a less favorable ratio of vestibular versus systemic toxicity. Interestingly, the difference in the balance between vestibular and systemic toxicity comparing the Swiss and the 129S1 strains following sub-chronic IDPN exposure is the opposite of that recorded following acute exposure (Boadas-Vaello et al., 2017). In the acute exposure model, 129S1 mice showed excessive systemic toxicity while Swiss mice provided a good model for vestibular toxicity studies. We hypothesize that these differences are due to variances in xenobiotic metabolism and therefore may be useful to address the pending question of the role of metabolic activation in the vestibular toxicity and other toxicities of this compound (Llorens and Crofton, 1991; Nace et al., 1997; Saldaña-Ruiz et al., 2012b).

The decline in vestibular function during sub-chronic IDPN exposure showed good reversibility if the exposure was terminated at 8 weeks, and all animals with VDRs  $\leq 15$  at that time recovered to low (0 to 2) values after 10-13 weeks of washout. This was consistent with the low to moderate alterations recorded at the SEM level in terms of stereociliary coalescence and HC loss. Moderate levels of vestibular dysfunction (VDRs in the 8 to 15 range) were associated with SEM Pathology Scores of 2 after washout, while lower VDRs (4 to 6) were associated with 0 to 1 SEM values. We concluded that significant loss of function can be observed in animals with no or minor loss of HCs, and that these animals allow the study of the

cellular and molecular events that precede HC loss and that associate with early and reversible vestibular dysfunction. In our previous rat study, irreversible vestibular dysfunction was associated with wider HC damage and loss (Sedó-Cabezón et al., 2015). In the present study, one single animal displayed deep dysfunction (VDR=18) and extensive damage (more than 50 % HCs missing or extruding in the utricle) so the association of this level of damage with irreversible dysfunction could not be addressed. However, the present mouse observations do not oppose the conclusion reached in the rat in which irreversible dysfunction is caused by HC loss.

In tissue sections examined by light microscopy and TEM, the coalescence of the stereociliary bundles, the displacement of the cytoplasm towards the side of the cell protruding into the endolymphatic cavity, and HCs extruded into that cavity were observed, matching with the SEM observations. HC extrusion has long been known to be the main form of HC demise occurring in the inner ear of birds and amphibians (Corwin et al., 1991; Cotanche, 1987). In mammals, HC extrusion has been recorded occasionally (e.g., Wersall et al., 1973; Granados and Meza, 2005), but very few investigations have specifically studied it. In a guinea pig aminoglycoside model, Li et al. (1995) showed a parallel occurrence of apoptotic and extruding HCs. However, our previous IDPN rat studies demonstrated that extrusion may appear as the only mode of HC demise (Seoane et al., 2001b; Sedó-Cabezón et al., 2015). We hypothesized that extrusion is the predominant form of HC demise during chronic ototoxic exposure in mammals (Seoane et al., 2001b); the present data supports this hypothesis by adding the mouse as a species where HC extrusion can appear as the predominant form of HC loss. While vacuolization was recorded in some HCs, no images suggestive of apoptosis were observed. Future work should decipher whether all ototoxic compounds, most notably the aminoglycosides, cause HC extrusion as the predominant form of HC loss if adequate exposure paradigms are used.

In addition to hair cell loss, other morphological and functional alterations have been described in the vestibular epithelia of mammals exposed to treatments causing incomplete damage. For instance, observations in an intratympanic gentamicin chinchilla model led Hirvonen et al. (2005) to conclude that calyceal retraction may be an important outcome of aminoglycoside exposure. In the present study, vestibular epithelia of IDPN exposed mice also displayed subtle alterations, such as the partial to complete absence of the electron densities that characterize the calyceal junction between HCl and calyx endings, accompanied by an increase in the membrane-to-membrane distances that revealed the dismantlement of the junction. Membrane-to-membrane distances are known to be reduced in the invaginations that occur between the calyx and the HCl (Lysakowski and Goldberg., 1997). However, our assessment did not include the comparison of the distances in the invaginations or of the number of invaginations. The width of extracellular spaces could hypothetically be modified by changes in osmolality (Lim et al., 2011), but there are no published data supporting that IDPN may affect osmolality. More relevant was the resemblance of the recorded increase in distances and loss of electron density to those reported to occur in Caspr1-null mice (Sousa et al., 2009). This effect of IDPN was observed in epithelia showing stereociliary abnormalities and HC extrusion but also in epithelia lacking these more prominent abnormalities, indicating that it constitutes an early event preceding the extrusion sequence. Importantly, it showed good, yet not fully complete, recovery in the washout animals. The dismantlement of the

calyceal junction and its rebuilding was further demonstrated by the immunofluorescent analysis of the expression of two proteins characterizing the junction, Caspr1 (Sousa et al., 2009; Lysakowski et al., 2011; Sedó-Cabezón et al., 2015) and Tenascin-C (Swartz and Santi, 1999; Lysakowski et al., 2011; Sedó-Cabezón et al., 2015). The loss of the calyceal proteins recorded in the confocal observations was not a secondary consequence of afferent retraction, because both TEM images and figures from NKA $\alpha$ 3 staining demonstrated the presence of the calyces in the absence of electron density and Caspr1 and Tenascin-C staining. Although alterations in calyx shape were indeed observed, the extent of the loss of the calyceal junctions exceeded by far that of the retraction of the calyces. Therefore, we hypothesize that dismantlement of the calyceal junction is an early step in the sequence of events finally leading up to HC extrusion. The possibility that this dismantlement is a direct effect of IDPN unrelated to HC extrusion cannot be excluded by the present data. However, the hypothesis that these are related events is simpler. Extrusion of the HCs, a phenomenon demonstrated to occur in other models (Li et al, 1995), ultimately requires detachment of the HCs from their neighboring cells, so an early loss of cell-to-cell contact is not a surprising step.

A role for the dismantlement and rebuilding of the calyceal junctions in the recorded loss and recovery of vestibular function can only be speculated. The junction has been proposed to have a prominent role in the synaptic transmission at the calyces. Data available indicate that it may contribute to non-quantal transmission by facilitating the accumulation of potassium or proton ions (Contini et al., 2012, 2017; Highstein et al., 2014; Lim et al., 2011). Other studies support the conclusion that the junction allows the accumulation of glutamate, leading to the stimulation of AMPA receptors located at farther distances from the point of release than those in typical synapses (Sadeghi et al., 2014). In any case, the calyceal junction would increase the firing probability of the afferent. In the IDPN animals with dismantled junctions, a decrease in afferent firing may be hypothesized to occur because of the increase in volume of the intercellular space deduced from the increase in membrane distances. While this hypothesis may be evaluated in future studies, additional questions remain open on the link between the present histological and behavioral data. Importantly, the calyces are hypothesized to signal high frequency events (Sadeghi et al., 2014), and the sensitivity of the behavioral test battery used here to evaluate these events has not been established.

A more direct insight into the basis of the reversible loss of vestibular function was provided by the Ribeye and GluA2 data. Overall, these data demonstrated that IDPN exposure caused a drop in synaptic elements that was reverted, but not in full, during washout. This evidence indicates that chronic ototoxicity causes synaptic uncoupling in the vestibular epithelium, and that this effect is reversible to different extents depending on the type of units considered. Thus, while recovery was complete in calyces from dimorphic afferents, incomplete recovery was recorded in calyx-only and HCII units. One important conclusion here is that the synaptic uncoupling occurs not only in the HCI-calyx contacts losing the calyceal junctions, but also in HCII-bouton contacts which do not have such junctions. The HCI effect matches the previous data in the rat (Sedó-Cabezón et al., 2015), while the effect in HCII had not been addressed in the rat model. The present data suggest that vestibular ganglion neurons suffer a significant drop in overall synaptic input during IDPN exposure, and this would account for the observed deficits in behavior. The fact that the recovery in synaptic puncta counts was not complete for calyx-only and HCII synapses contrasts with the apparent completeness of the behavioral

recovery. However, recovery was complete in synapses of dimorphic afferent calyces, and the sensitivity of the recorded behaviors to small synaptic alterations has not been established. The function of the diverse HC and neuronal types in the vestibular system and the behavioral correlates of their diversity are far from being understood, and only in recent years have these questions begun to be addressed (e.g., Curthoys et al., 2014). Future studies may more precisely relate the persistent or reversible alterations in synapses to specific physiological outcomes. However, there is still a scarcity of robust and quantitative models to evaluate the different vestibular functions (Llorens et al., 2018).

The expression of Tenascin-C in the calyceal junction has been described (Swartz and Santi, 1999; Warchol and Speck, 2007; Lysakowski et al., 2011), but whether this extracellular protein is secreted by the HC or the neuron is not established. The large difference in Tnc mRNA expression between the vestibular epithelium and the ganglion suggest that the HC, not the neuron, secretes this protein to the extracellular space at the calyceal contact. The expression data showed that decreased Tnc and CtBP2 expression occur in parallel with the observed changes in Tenascin-C and Ribeye/CtBP2 protein expression. This suggests that HCs under toxic stress trigger a genetic program for calyceal junction dismantlement and synaptic uncoupling. After washout, complete recovery in Tenascin-C protein expression and Tnc gene expression was recorded and in agreement with the TEM observations of calyceal junction rebuilding. In contrast, Ribeye puncta numbers in some synaptic types and Ctbp2 mRNA expression in the epithelium remained altered after washout, indicating that HCs may suffer defective recovery, at least for long periods of time after the end of the exposure. In the vestibular ganglion containing the post-synaptic neurons, the expression of the Cntnap1 gene, encoding Caspr1, was not significantly altered. This result, similar to that previously obtained in the rat (Sedó-Cabezón et al., 2015), suggests that the vestibular ganglion neurons may not drive the dismantlement of the calyceal junction at the gene expression level. However, it may have an active role in synaptic uncoupling. In the rat model, we recorded a small but significant decrease in Gria2 expression after exposure (Sedó-Cabezón et al., 2015), while a small non-significant decrease was recorded in the mouse. The present results neither confirm nor oppose the previous data. Finally, the significant increase in Gria2 expression in the washout mice reinforces the notion that persistent molecular alterations may persist in the system long after the end of the toxic exposure period.

In addition to the vestibular toxicity, IDPN is well known to cause neurofilamentous proximal axonopathy (Chou and Hartmann, 1964; Griffin et al., 1978; Llorens, 2013). However, these effects are likely independent, as they show different dose-response and time-course relationships (Llorens and Rodríguez-Farré, 1997). This conclusion is strongly supported by the fact that other nitriles, including allylnitrile and cis-crotononitrile, cause vestibular toxicity (Balbuena and Llorens, 2001, 2003; Boadas-Vaello et al., 2007, 2009; Rúa et al., 2013) but are not axonopathic (Soler-Martín et al., 2011). Although a role for the axonopathic effect of IDPN in the dismantlement of the calyceal junction and synaptic uncoupling cannot be completely excluded, the congruent alterations found in the pre- and post-synaptic sides, and the evidence of the involvement of gene expression changes in the HC response, strongly support that these are phenomena occurring in response to the chronic ototoxic stress, not a secondary effect of the neurofilamentous axonopathy. Future studies using other chronic ototoxicity models are needed to differentiate between the effects that are common to all

models and those that are particular to IDPN. Interestingly, recent data (Sultemeier and Hoffman, 2017) demonstrate that alterations in the afferents may occur in vestibular epithelia exposed to ototoxic agents at exposure regimes milder than those causing widespread HC loss. These authors used low-dose intra-labyrinth injection of gentamicin in the chinchilla and found that persistent alterations in the calyx afferents occurred together with the continued presence of the corresponding HCs. As the model and methods used by Sultemeier and Hoffman (2017) differ greatly from the ones used here, it is unclear whether the present data and their data reveal similar or distinct phenomena.

In summary, we developed a model to study the early stages of chronic vestibular toxicity in the mouse. In this model, vestibular dysfunction preceded HC loss, and this early loss of function largely reversed if the exposure was terminated. At these early stages of chronic ototoxicity, a dismantlement of the calyceal junctions between HCI and calyx afferents occurred, and this effect showed good reversibility. Another prominent feature was synaptic uncoupling, with a reversibility that varied depending on the type of synaptic unit considered. Toxicity progressed through HC loss via extrusion of HCs towards the endolymphatic cavity. Taken together, the present data delineate the sequence of events shown in Fig. 7 for loss of HCIs. Calyceal junction dismantlement cannot affect the junction-less HCIs, but synaptic uncoupling was demonstrated in these cells as well. We also obtained data supporting that these changes may be driven, at least in part, by changes in gene expression. This mouse model should be useful to study the molecular basis of the vestibular deficits arising during chronic ototoxicity.

**Conflict of Interest:** The authors declare that they have no conflict of interest

## REFERENCES

- Balbuena E, Llorens J (2001) Behavioural disturbances and sensory pathology following allylnitrile exposure in rats. *Brain Res* 904: 298-306.
- Balbuena E, Llorens J (2003) Comparison of cis- and trans-crotonitrile effects in the rat reveals specificity in the neurotoxic properties of nitrile isomers. *Toxicol Appl Pharmacol* 187: 89-100.
- Black FO, Gianna-Poulin C, Pesznecker SC (2001) Recovery from vestibular ototoxicity. *Otol Neurotol* 22: 662-671.
- Black FO, Pesznecker S, Stallings V (2004) Permanent gentamicin vestibulotoxicity. *Otol Neurotol* 25: 559-569.
- Boadas-Vaello P, Jover E, Díez-Padrisa N, Bayona JM, Llorens J (2007) Differential role of CYP2E1-mediated metabolism in the lethal and vestibulotoxic effects of cis-crotonitrile in the mouse. *Toxicol Appl Pharmacol* 225: 310-317.
- Boadas-Vaello P, Jover E, Saldaña-Ruiz S, Soler-Martín C, Chabbert C, Bayona JM, Llorens J (2009) Allylnitrile metabolism by CYP2E1 and other CYPs leads to distinct lethal and vestibulotoxic effects in the mouse. *Toxicol Sci* 107: 461-472.
- Boadas-Vaello P, Riera J, Llorens J (2005) Behavioral and pathological effects in the rat define two groups of neurotoxic nitriles. *Toxicol Sci* 88: 456-466.
- Boadas-Vaello P, Sedó-Cabezón L, Verdú E, Llorens J (2017) Strain and sex differences in the vestibular and systemic toxicity of 3,3'-iminodipropionitrile in mice. *Toxicol Sci* 156: 109-122.
- Breglio AM, Rusheen AE, Shide ED, Fernandez KA, Spielbauer KK, McLachlin KM, Hall MD, Amable L, Cunningham LL (2017) Cisplatin is retained in the cochlea indefinitely following chemotherapy. *Nat Commun* 8: 1654.
- Callejo A, Durochat A, Bressieux S, Saleur A, Chabbert C, Domènech Juan I, Llorens J, Gaboyard-Niay S (2017) Dose-dependent cochlear and vestibular toxicity of trans-tympanic cisplatin in the rat. *Neurotoxicology* 2017; 60: 1-9.
- Chou SM, Hartmann HA (1964) Axonal lesions and waltzing syndrome after IDPN administration in rats. With a concept—Axostasis. *Acta Neuropathol* 3: 428-450.
- Contini D, Price SD, Art JJ (2017) Accumulation of K<sup>+</sup> in the synaptic cleft modulates activity by influencing both vestibular hair cell and calyx afferent in the turtle. *J Physiol* 595: 777-803.
- Contini D, Zampini V, Tavazzani E, Magistretti J, Russo G, Prigioni I, Masetto S (2012) Intercellular K<sup>+</sup> accumulation depolarizes Type I vestibular hair cells and their associated afferent nerve calyx. *Neuroscience* 227: 232-246.
- Corwin JT, Jones JE, Katayama A, Kelley MW, Warchol ME (1991) Hair cell regeneration: the identities of progenitor cells, potential triggers and instructive cues. *Ciba Found Symp* 160: 103-120.

Crofton KM, Janssen R, Prazma J, Pulver S, Barone Jr.S (1994) The ototoxicity of 3,3'-iminodipropionitrile: Functional and morphological evidence of cochlear damage. *Hear Res* 80: 129-140

Cotanche DA (1987) Regeneration of hair cell stereociliary bundles in the chick cochlea following severe acoustic trauma. *Hear Res* 30: 181-195.

Curthoys IS, Vulovic V, Burgess AM, Manzari L, Sokolic L, Pogson J, Robins M, Mezey LE, Goonetilleke S, Cornell ED, MacDougall HG (2014) Neural basis of new clinical vestibular tests: otolithic neural responses to sound and vibration. *Clin Exp Pharmacol Physiol* 41: 371-380.

Dechesne C, Mbiene JP, Sans A (1986) Postnatal development of vestibular receptor surfaces in the rat. *Acta Otolaryngol* 101: 11-18.

Desai SS, Ali H, Lysakowski A (2005) Comparative morphology of rodent vestibular periphery. II. Cristae ampullares. *J Neurophysiol* 93: 267-280.

Gaboyard-Niay S, Travo C, Saleur A, Broussy A, Brugeaud A, Chabbert C (2016) Correlation between afferent rearrangements and behavioral deficits after local excitotoxic insult in the mammalian vestibule: a rat model of vertigo symptoms. *Dis Model Mech* 9: 1181-1192.

Gagnaire F, Marignac B, Ban M, Langlais C (2001) The ototoxic effects induced in rats by treatment for 12 weeks with 2-butenenitrile, 3-butenenitrile and cis-2-pentenenitrile. *Pharmacol Toxicol* 88: 126-134.

Golub JS, Tong L, Ngyuen TB, Hume CR, Palmiter RD, Rubel EW, Stone JS (2012) Hair cell replacement in adult mouse utricles after targeted ablation of hair cells with diphtheria toxin. *J Neurosci* 32: 15093-15105.

Goodyear RJ, Gale JE, Ranatunga KM, Kros CJ, Richardson GP (2008) Aminoglycoside-induced phosphatidylserine externalization in sensory hair cells is regionally restricted, rapid, and reversible. *J Neurosci* 28: 9939-9952.

Granados O, Meza G (2005) Streptidine, a metabolic derivative produced after administration of streptomycin in vivo, is vestibulotoxic in rats. *Histol Histopathol* 20: 357-364.

Griffin JW, Hoffman PN, Clark AW, Carroll PT, Price DL (1978) Slow axonal transport of neurofilament proteins: Impairment by 3,3'-iminodipropionitrile administration. *Science* 202: 633-635.

Highstein SM, Holstein GR, Mann MA, Rabbitt RD (2014) Evidence that protons act as neurotransmitters at vestibular hair cell-calyx afferent synapses. *Proc Natl Acad Sci U S A* 111: 5421-5426.

Hirvonen TP, Minor LB, Hullar TE, Carey JP (2005) Effects of intratympanic gentamicin on vestibular afferents and hair cells in the chinchilla. *J Neurophysiol* 93:643-655.

Hodgkinson L, Prasher D (2006) Effects of industrial solvents on hearing and balance: a review. *Noise Health* 8: 114-133.

- Li L, Nevill G, Forge A (1995) Two modes of hair cell loss from the vestibular sensory epithelia of the guinea pig inner ear. *J Comp Neurol* 355: 405-417.
- Li Y, Ding D, Jiang H, Fu Y, Salvi R (2011) Co-administration of cisplatin and furosemide causes rapid and massive loss of cochlear hair cells in mice. *Neurotox Res* 20: 307-319.
- Lim R, Kindig AE, Donne SW, Callister RJ, Brichta AM (2011) Potassium accumulation between type I hair cells and calyx terminals in mouse crista. *Exp Brain Res* 210: 607-621.
- Llorens J (2013) Toxic neurofilamentous axonopathies - accumulation of neurofilaments and axonal degeneration. *J Intern Med* 273: 478-489.
- Llorens J, Aguiló A, Rodríguez-Farré E (1998) Behavioral disturbances and vestibular pathology following crotonitrile exposure in rats. *J Periph Nerv Sys* 3: 189-196.
- Llorens J, Callejo A, Greguske EA, Maroto AF, Cutillas B, Martins-Lopes V (2018) Physiological assessment of vestibular function and toxicity in humans and animals. *Neurotoxicology* 66: 204-212.
- Llorens J, Crofton KM (1991) Enhanced neurotoxicity of 3,3'-iminodipropionitrile following carbon tetrachloride pretreatment in the rat. *Neurotoxicology* 12: 583-594.
- Llorens J, Demêmes D, Sans A (1993) The behavioral syndrome caused by 3,3'-iminodipropionitrile and related nitriles in the rat is associated with degeneration of the vestibular sensory hair cells. *Toxicol Appl Pharmacol* 123: 199-210.
- Llorens J, Rodríguez-Farré E (1997) Comparison of behavioral, vestibular, and axonal effects of subchronic IDPN in the rat. *Neurotoxicol Teratol* 19: 117-127.
- Lysakowski A, Gaboyard-Niay S, Calin-Jageman I, Chatlani S, Price SD, Eatock RA (2011) Molecular microdomains in a sensory terminal, the vestibular calyx ending. *J Neurosci* 31: 10101-10114.
- Lysakowski A, Goldberg JM (1997) A regional ultrastructural analysis of the cellular and synaptic architecture in the chinchilla cristae ampullares. *J Comp Neurol* 389: 419-443.
- McCall AA, Yates BJ (2011) Compensation following bilateral vestibular damage. *Front Neurol* 2, 88.
- Murillo-Cuesta S, Contreras J, Cediell R, Varela-Nieto I (2010) Comparison of different aminoglycoside antibiotic treatments to refine ototoxicity studies in adult mice. *Lab Anim* 44: 124-131.
- Nace CG, Genter MB, Sayre LM, Crofton KM (1997) Effect of methimazole, an FMO substrate and competitive inhibitor, on the neurotoxicity of 3,3'-iminodipropionitrile in male rats. *Fundam Appl Toxicol* 37: 131-140.
- Oesterle EC, Campbell S, Taylor RR, Forge A, Hume CR (2008) Sox2 and JAGGED1 expression in normal and drug-damaged adult mouse inner ear. *J Assoc Res Otolaryngol* 9: 65-89.

- Op de Beeck K, Schacht J, Van Camp G (2011) Apoptosis in acquired and genetic hearing impairment: the programmed death of the hair cell. *Hear Res* 281: 18-27.
- Paken J, Govender CD, Pillay M, Sewram V (2016) Cisplatin-associated ototoxicity: A review for the health professional. *J Toxicol*. <https://doi.org/10.1155/2016/1809394>
- Rúa F, Buffard M, Sedó-Cabezón L, Hernández-Mir G, de la Torre A, Saldaña-Ruiz S, Chabbert C, Bayona JM, Messeguer A, Llorens J (2013) Vestibulotoxic properties of potential metabolites of allylnitrile. *Toxicol Sci* 135: 182-192.
- Ruan Q, Ao H, He J, Chen Z, Yu Z, Zhang R, Wang J, Yin S (2014) Topographic and quantitative evaluation of gentamicin-induced damage to peripheral innervation of mouse cochleae. *Neurotoxicology* 40: 86-96.
- Rubel EW, Furrer SA, Stone JS (2013) A brief history of hair cell regeneration research and speculations on the future. *Hear Res* 297: 42-51.
- Sadeghi SG, Pyott SJ, Yu Z, Glowatzki E (2014) Glutamatergic signaling at the vestibular hair cell calyx synapse. *J Neurosci* 34: 14536-14550.
- Saldaña-Ruiz S, Boadas-Vaello P, Sedó-Cabezón L, Llorens J (2013) Reduced systemic toxicity and preserved vestibular toxicity following co-treatment with nitriles and CYP2E1 inhibitors: a mouse model for hair cell loss. *J Assoc Res Otolaryngol* 14: 661-671.
- Saldaña-Ruiz S, Hernández-Mir G, Sedó-Cabezón L, Cutillas B, Llorens J (2012a) Vestibular toxicity of cis-2-pentenenitrile in the rat. *Toxicol Lett* 211: 281–288.
- Saldaña-Ruiz S, Soler-Martín C, Llorens J (2012b) Role of CYP2E1-mediated metabolism in the acute and vestibular toxicities of nineteen nitriles in the mouse. *Toxicol Lett* 208: 125-132.
- Schacht J, Talaska AE, Rybak LP (2012) Cisplatin and aminoglycoside antibiotics: hearing loss and its prevention. *Anat Rec* 295: 1837-1850.
- Schuth O, McLean WJ, Eatock RA, Pyott SJ (2014) Distribution of Na,K-ATPase  $\alpha$  subunits in rat vestibular sensory epithelia. *J Assoc Res Otolaryngol* 15: 739-754.
- Sedó-Cabezón L, Boadas-Vaello P, Soler-Martín C, Llorens J (2014) Vestibular damage in chronic ototoxicity: a mini-review. *Neurotoxicology* 43: 21-27.
- Sedó-Cabezón L, Jedynek P, Boadas-Vaello P, Llorens J (2015) Transient alteration of the vestibular calyceal junction and synapse in response to chronic ototoxic insult in rats. *Dis Model Mech* 8: 1323-1337.
- Seoane A, Demêmes D, Llorens J (2001a). Pathology of the rat vestibular sensory epithelia during subchronic 3,3'-iminodipropionitrile exposure: hair cells may not be the primary target of toxicity. *Acta Neuropathol* 102: 339-348.
- Seoane A, Demêmes D, Llorens J (2001b). Relationship between insult intensity and mode of hair cell loss in the vestibular system of rats exposed to 3,3'-iminodipropionitrile. *J Comp Neurol* 439: 385-399.

Shi X, Gillespie PG, Nuttall AL (2005) Na<sup>+</sup> influx triggers bleb formation on inner hair cells. *Am J Physiol Cell Physiol* 288: C1332-C1341.

Soler-Martín C, Boadas-Vaello P, Saldaña-Ruíz S, Cutillas B, Llorens J (2011) Butenenitriles have low axonopathic potential in the rat. *Toxicol Lett* 200: 187-193.

Soler-Martín C, Diez-Padrisa N, Boadas-Vaello P, Llorens J (2007) Behavioral disturbances and hair cell loss in the inner ear following nitrile exposure in mice, guinea pigs, and frogs. *Toxicol Sci* 96: 123-132.

Sousa AD, Andrade LR, Salles FT, Pillai AM, Buttermore ED, Bhat MA, Kachar B (2009) The septate junction protein caspr is required for structural support and retention of KCNQ4 at calyceal synapses of vestibular hair cells. *J Neurosci* 29: 3103-3108.

Sultemeier DR, Hoffman LF (2017) Partial aminoglycoside lesions in vestibular epithelia reveal broad sensory dysfunction associated with modest hair cell loss and afferent calyx retraction. *Front Cell Neurosci* 11: 331.

Swartz DJ, Santi PA (1999) Immunolocalization of tenascin in the chinchilla inner ear. *Hear Res* 130: 108-114.

Tanii H, Takayasu T, Higashi T, Leng S, Saijoh K (2004) Allylnitrile: generation from cruciferous vegetables and behavioral effects on mice of repeated exposure. *Food Chem Toxicol* 42: 453-458.

Taylor RR, Jagger DJ, Saeed SR, Axon P, Donnelly N, Tysome J, Moffatt D, Irving R, Monksfield P, Coulson C, Freeman SR, Lloyd SK, Forge A (2015) Characterizing human vestibular sensory epithelia for experimental studies: new hair bundles on old tissue and implications for therapeutic interventions in ageing. *Neurobiol Aging* 36: 2068-2084.

Taylor RR, Nevill G, Forge A (2008) Rapid hair cell loss: a mouse model for cochlear lesions. *J Assoc Res Otolaryngol* 9: 44-64.

Warchol ME, Speck JD (2007) Expression of GATA3 and tenascin in the avian vestibular maculae: normative patterns and changes during sensory regeneration. *J Comp Neurol* 500: 646-657.

Wersäll J, Björkroth B, Flock A, Lundquist PG (1973) Experiments on ototoxic effects of antibiotics. *Adv Otorhinolaryngol* 20: 14-41.

Wu WJ, Sha SH, McLaren JD, Kawamoto K, Raphael Y, Schacht J (2001) Aminoglycoside ototoxicity in adult CBA, C57BL and BALB mice and the Sprague-Dawley rat. *Hear Res* 158: 165-178.

## Figure Legends

Figure 1: Effects of IDPN (30 mM in the drinking water) on body weight and vestibular function of male 129S1/SvImJ mice. In both panels, the line at the bottom of the graph indicates the 8-week exposure period. A: Body weight. Numbers of animals changed at the end of the 8-week exposure period, from 21 controls and 43 treated on the left side to 9 controls and 17 treated on the right side. B: Vestibular Dysfunction Ratings. Data are sum ratings from a battery of 6 tests sensitive to vestibular dysfunction, each rated 0 (normal behavior) to 4 (extreme evidence of vestibular loss). Numbers of animals changed at the end of the 8-week exposure period, from 13 controls and 27 treated on the left side to 7 controls and 13 treated on the right side. \*: Significantly different ( $p < 0.05$ ), Duncan's tests after significant repeated-measures MANOVA.

Figure 2: Effects of IDPN (30 mM in the drinking water) on the utricle as assessed by SEM analysis of the surfaces of the sensory epithelia. Except in F, all images correspond to the central (peri-striolar) part of the utricle. (A) Control mouse. A uniform distribution of stereociliary bundles emerging from a field of microvilli indicate a normal density of HCs. (B-G) Utricles from mice exposed to IDPN for 8 weeks with diverse pathological stages. (B) Utricle with a SEM Pathology score of 0 from a mouse with a VDR of 4. (C) Utricle with a SEM Pathology score of 2 from a mouse with a VDR of 10; note the presence of coalescent hair bundles (arrows). (D-E) Details of an utricle with a SEM pathology score of 3 from a mouse with a VDR of 10, showing a lack of HCs (asterisks in D) and extruding HCs (arrowheads in E). (F) Utricle of the worst-case mouse, displaying a VDR of 18 and a SEM pathology score of 4, with widespread loss of and ongoing extrusion of HCs. (G) Higher magnification of the area defined by the white rectangle in F. (H-J) Utricles from mice exposed to IDPN for 8 weeks and studied after a washout period of 13 weeks. In I and J, asterisks signal spaces lacking a HC, and arrows signal coalescent stereociliary bundles. (H) SEM Pathology Score of 0 in a mouse presenting a VDR of 6 at 8 weeks, and a VDR of 1 after washout. (I) SEM Pathology Score of 2 in a mouse presenting a VDR of 8 at 8 weeks, and a VDR of 1 after washout. (J) SEM Pathology Score of 2 in a mouse presenting a VDR of 15 at 8 weeks, and a VDR of 1 after washout. (K) Relationship between VDRs at the end of the exposure period and SEM Pathology Scores in control mice (circles) and in mice exposed to 30 mM IDPN for 5 (squares) or 8 (triangles) weeks; animals were examined by SEM at the end of the exposure (black symbols) or after a washout period (light grey symbols). (L) Relationship between SEM Pathology Scores assessed after washout and VDR recovery in mice exposed to 0 (circles) or 30 (triangles) mM IDPN for 8 weeks. Each animal is represented by two symbols showing the VDR at the end of the exposure period (black), and at the end of the washout (light gray). Note that animals with a pathology score of 2, that is, showing only minimal evidence of HC loss or damage, had shown moderate dysfunction ratings (8 to 15) at the end of the exposure period, and complete recovery (ratings of 1 to 2) after washout. Scale bars: 10  $\mu\text{m}$  in A, B, C, G, H, I and J; 5  $\mu\text{m}$  in D and E; 250  $\mu\text{m}$  in F.

Figure 3: Effects of IDPN (30 mM in the drinking water) on the lateral vestibular crista as assessed by light microscopy (J) and TEM (all other images). (A-C) Control epithelium. Note the calyceal afferent endings (c in A and C, one of them highlighted in green) encasing type I hair cells (HCI). Supporting cells (sc) fill the basal end of the epithelium and extend their apical

processes separating the HCs. In B, note type II hair cells (HCII) contacted by bouton afferents (b, also highlighted in green). In the higher magnification image in C, note the difference in electron density of the membranes in the calyceal junction area (arrows) compared to other plasma membranes elsewhere in the epithelium (arrowheads). (D) Crista from a mouse exposed to IDPN for 5 weeks. In this HCl-afferent contact, the calyx ending (c) is fragmented and does not cover the bottom end of the HCl (asterisks) as it should. The calyceal junction is missing in most of the area where the calyx continues covering the HCl (arrowheads). (E) Representative image of a crista from a mouse exposed to IDPN for 8 weeks. In this HCl-calyx afferent contact, the calyceal junction is observed in some segments (arrows) and is lacking in others (arrowheads). (F) Extruding HCl in a mouse exposed to IDPN for 8 weeks. Note the calyx afferent (c), and the kinocilium (arrow). (G) Extruding cells in the crista from the worst-case example animal exposed to IDPN for 8 weeks. Note the remnants of a completely extruded cell (arrow) in the endolymphatic cavity. (I): Extensive vacuolization in a partially extruded HC, from the same crista shown in G.(I): Representative image of crista after a washout period of 13 weeks. The calyceal junctions are distinctly visible in most basolateral membranes of the HCl. (J) High magnification image of a calyceal junction in a control mouse. The three marks show the membrane-to-membrane distances, which are small and uniform. (K) High magnification image of a membrane region where a calyceal junction has been lost in a mouse exposed to IDPN for 8 weeks. Note the increase in membrane-to-membrane distances and their reduced uniformity. (L): Mean membrane-to-membrane distances including all points throughout the HCl-calyx contact. Data are  $X \pm SE$  from 1,285 (control), 1047 (8 week of IDPN), and 1242 (washout) points. a, b, c: groups signaled with different letters are significantly different from each other,  $P < 0.05$ , Duncan's test after significant ANOVA. Scale bars: 10  $\mu\text{m}$  in A, B and G; 2  $\mu\text{m}$  in C, D, E, F, H and I; 100 nm in J and K.

Figure 4: Effects of IDPN (30 mM in the drinking water for 8 weeks) and washout (13 weeks) on the expression of calyceal junction proteins. (A) Representative images of the cristae immunolabeled with anti-NaKA $\alpha$ 3 (red), anti-Caspr1 (green) and anti-Tenascin-C (blue) antibodies. In the overlay figures, yellow and white indicates overlapping signals at this level of resolution. (a-d) Control. The anti-NaKA $\alpha$ 3 antibody labels the entire membrane of the afferent endings. The cup-shaped green and blue labeling correspond to the known localization of Caspr1 in the inner face of the calyx membrane and Tenascin-C in the extracellular space, both at the calyceal junction area. Caspr1 expression is similar in all calyces, while Tenascin-C expression is markedly higher in the calyces from the central part compared to those in the peripheral part of the crista. (e-h) After exposure to IDPN for eight weeks, labeling of Caspr1 and Tenascin-C is markedly reduced, while NaKA $\alpha$ 3 label is maintained. (i-l) After a 13-week washout period, an extensive recovery in Caspr1 and Tenascin-C labeling was observed. The scale bar in l is 25  $\mu\text{m}$  long and applies to all panels. (B) Number of identifiable Caspr1, Tenascin-C, and colocalization cup-shaped label profiles. Data are  $X \pm SE$  counts from 6 control, 3 IDPN, and 5 washout (WO) mice. a, b, c: groups signaled with different letters are significantly different from each other,  $P < 0.05$ , Duncan's test after significant ANOVA. (C) Schema of the vestibular epithelium showing the localization of the NaKA $\alpha$ 3 (red), Caspr1 (green), and Tenascin-C (blue) labels.

Figure 5: Effects of IDPN (30 mM in the drinking water for 8 weeks) and washout (13 weeks) on the expression of synaptic proteins. (A) Representative images of the cristae immunolabeled

with anti-Ribeye/CtBP2 antibody (red), anti-GluA2 (green), and anti-Calretinin (blue). In the overlay figures, yellow and white indicates overlapping signals at this level of resolution. The asterisks in (a) and (b) indicate a blood vessel revealed by the anti-mouse secondary antibodies. This unspecific staining did not interfere with the specific labels. (a-d) Control. (a) The anti-Ribeye/CtBP2 antibody labels the CtBP2 transcription factor in the nuclei of HCs (arrowhead) and supporting cells, and the Ribeye protein in the ribbon synapses of the HCs, appearing as a punctate label (arrow) between the rows of the HC nuclei and supporting cell nuclei. (b) The anti-GluA2 antibody labels the AMPA-type glutamate receptor clusters in the postsynaptic membranes, appearing as a punctate label (arrow). (c) The anti-calretinin antibody labels calyx-only afferents (arrow), and a subset of HC, most of which are HCII (arrowhead). (e-h) After exposure to IDPN for 8 weeks, there was a noticeable reduction in Ribeye and GluA2 puncta. (i-l) After a 13-week washout period, some recovery in Ribeye and GluA2 puncta was recorded. (m and n) Larger views of the boxed areas in d and h, respectively. (m-n) Representative high magnification views of a dimorphic (o) and a calretinin-positive HCII (p) showing pre-synaptic (ribeye) and post-synaptic (GluA2) puncta and their colocalization. In each cell, two paired puncta are signaled by an arrow and an arrowhead. The scale bar in l is 25  $\mu\text{m}$  long and applies to panels a-l, that in n is 5  $\mu\text{m}$  long and applies to panels m-n, and that in p is 5  $\mu\text{m}$  long and applies to panels o-p. (B) Quantitative analysis of number of Ribeye and GluA2 puncta and their colocalizations, by unit type. Data are  $\bar{X} \pm \text{SE}$  counts from 169 cells from 9 control animals, 147 cells from 5 IDPN 8-week animals, and 188 cells from 6 washout (WO) animals. a, b, c: groups not sharing a letter are significantly different,  $P < 0.05$ , Duncan's test after significant ANOVA. Absence of letters indicates lack of group differences by ANOVA.

Figure 6: RT-PCR of mRNA from vestibular epithelium or ganglia displays significantly altered expression of *Tnc*, *Ctbp2*, and *Gria2* but unchanged for *Caspr1* ( $n=8-9$  per group). a, b: groups signaled with different letters are significantly different from each other,  $P < 0.05$ , Duncan's test after significant ANOVA. Absence of letters in the *Cntnap1* comparison indicates lack of group differences by ANOVA.

Figure 7: Schema of the steps involved in HC demise during chronic vestibular IDPN toxicity. A single HCI is represented. The earliest identified step includes dismantlement of the calyceal junction, with loss of *Caspr1* and *Tenascin-C*, and synaptic uncoupling, with a decrease in Ribeye and GluA2 puncta. This early step is largely reversible. Progressing damage involves ciliary coalescence and HC extrusion. An unidentified point of no return is hypothesized. HCII do not have calyceal junctions, but they similarly show synaptic uncoupling, ciliary coalescence and extrusion.

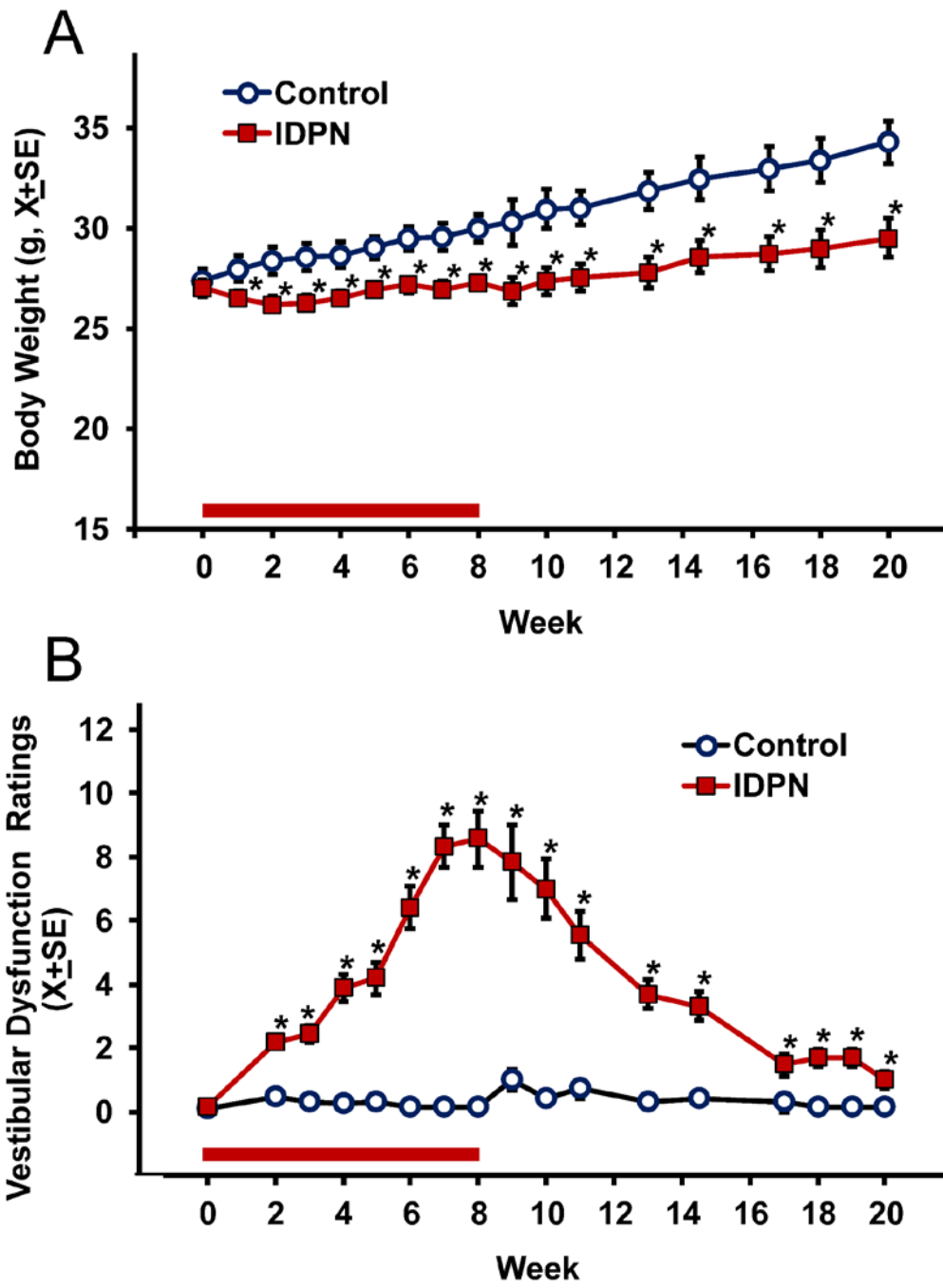


Figure 1

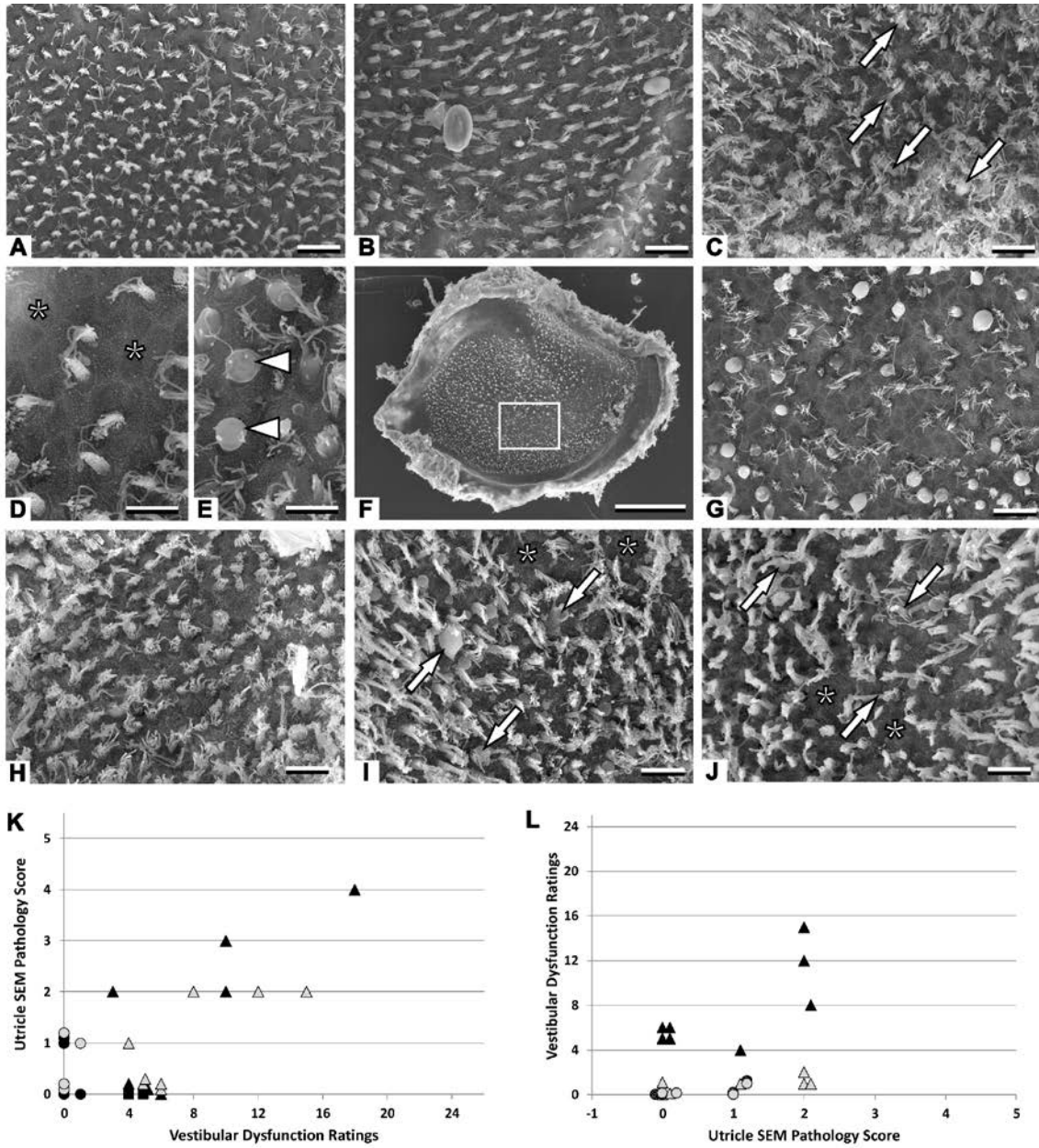


Figure 2

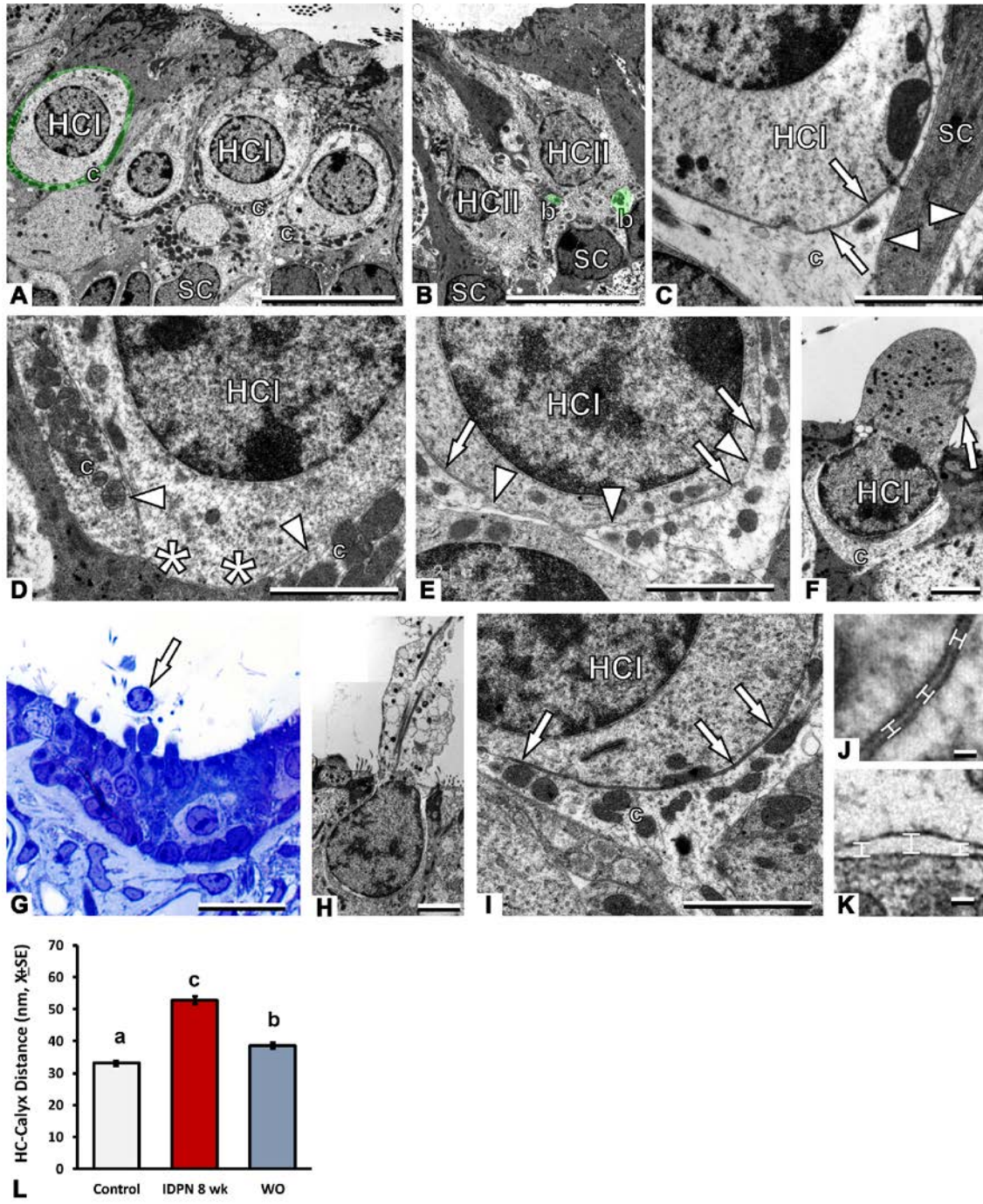


Figure 3

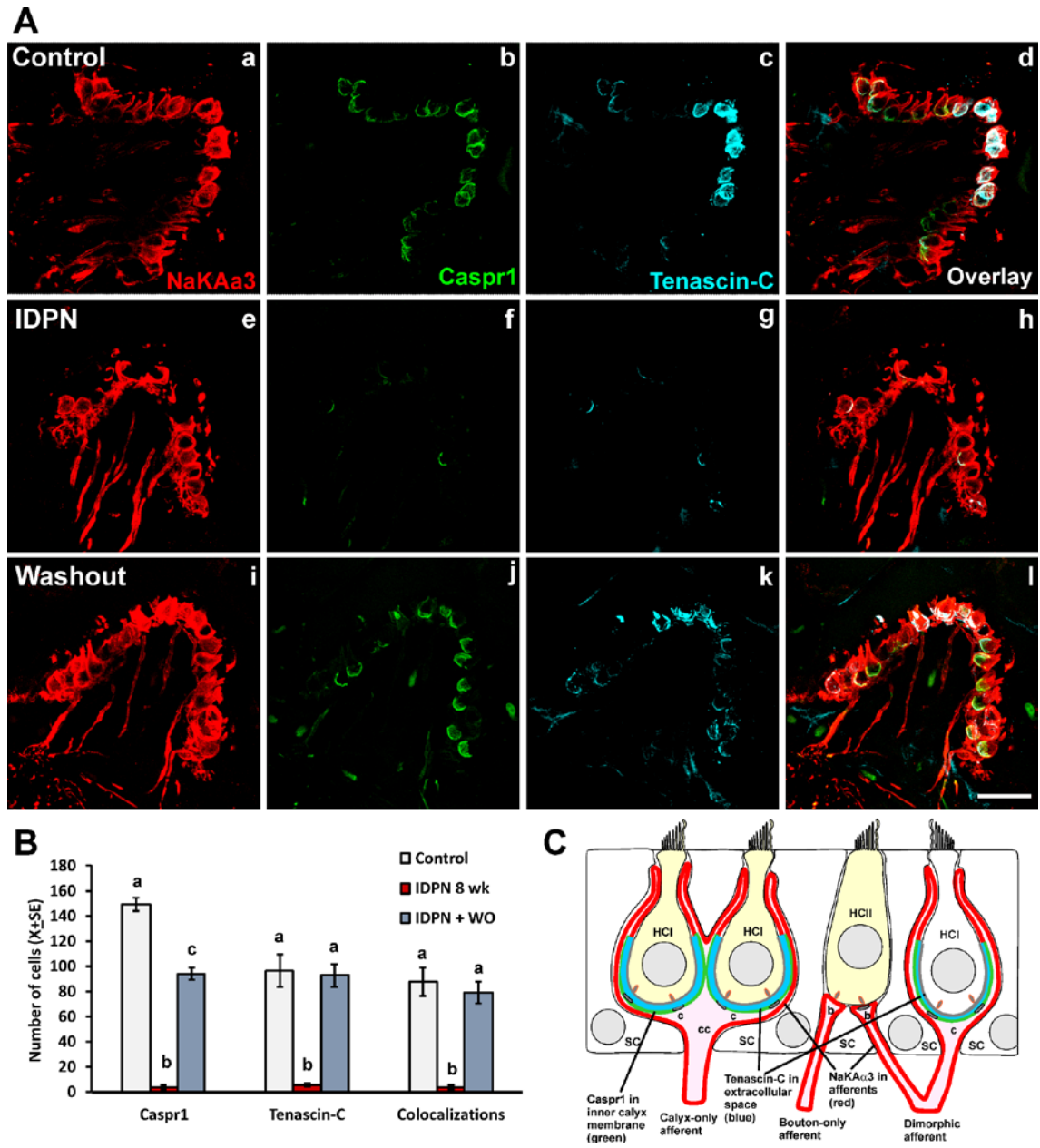


Figure 4

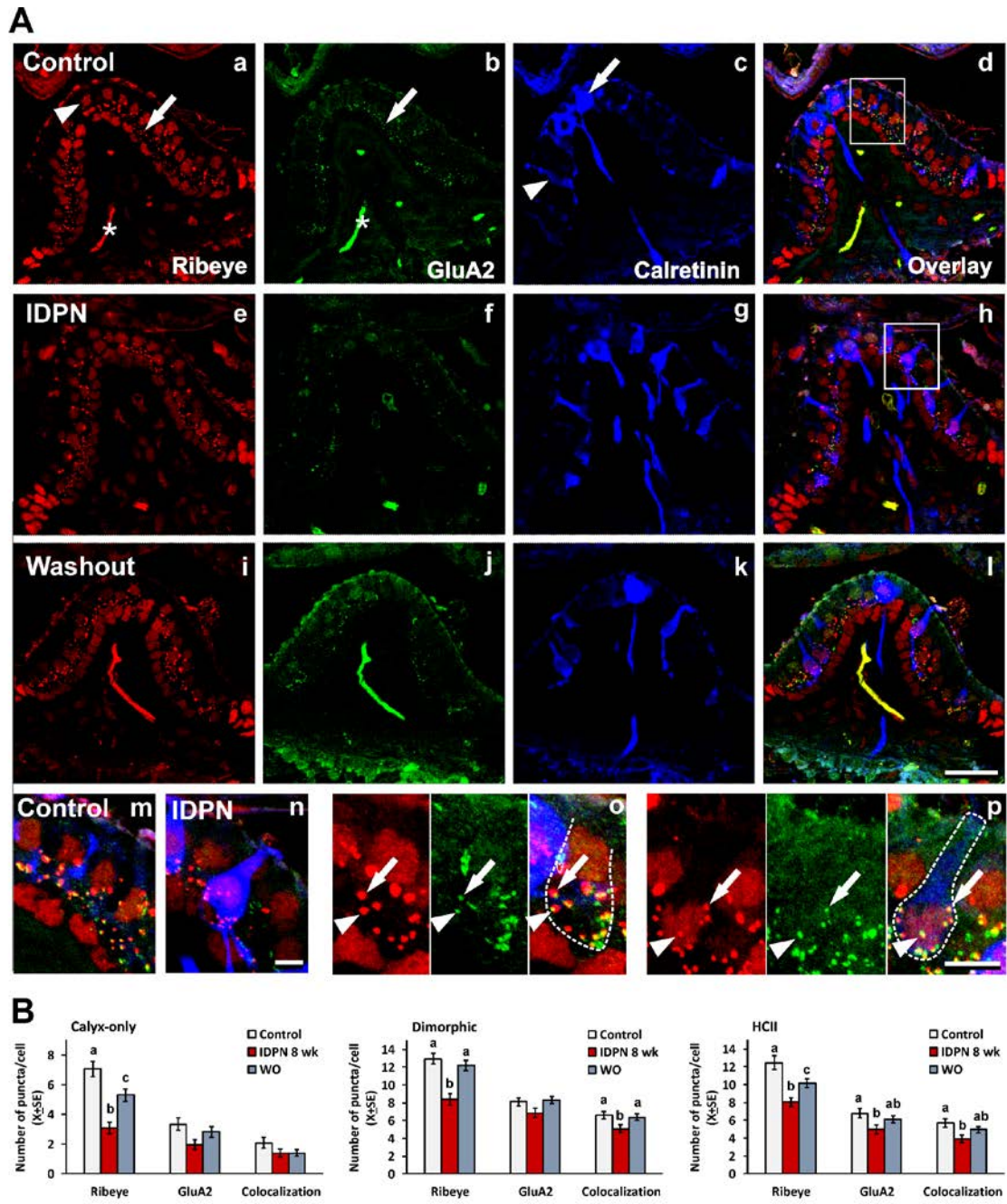


Figure 5

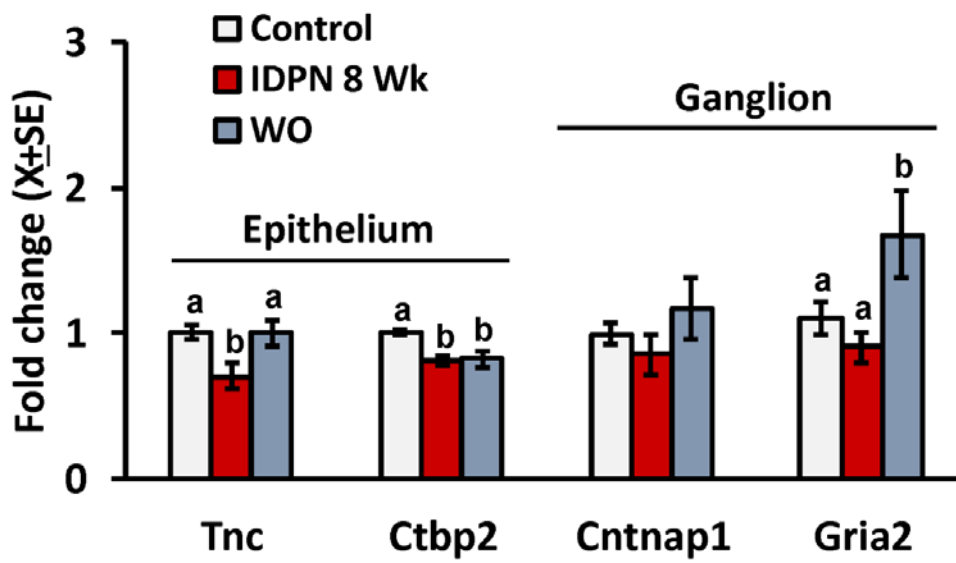


Figure 6

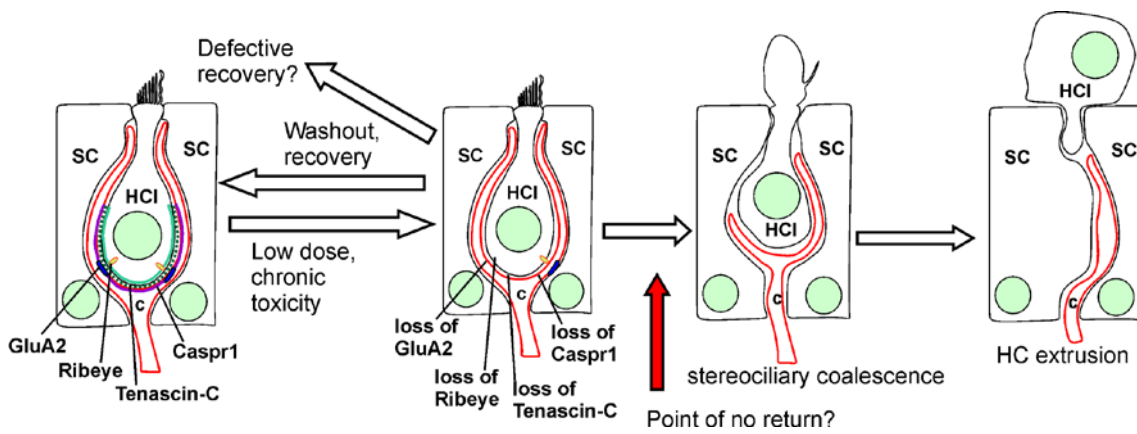


Figure 7

## **Supplementary Methods and Figure Legends**

Erin A. Greguske, Maria Carrerres-Pons, Blanca Cutillas, Pere Boadas-Vaello, Jordi Llorens

### **Calyx junction dismantlement and synaptic uncoupling precede hair cell extrusion in the vestibular sensory epithelium during sub-chronic 3,3'-iminodipropionitrile ototoxicity in the mouse**

#### **Supplementary Methods**

Preliminary experiments evaluated the suitability of mice of different sex and strain [129S1/SvImJ (129S1) and RjOrl:Swiss/CD-1 (Swiss)] to study sub-chronic vestibular toxicity using the IDPN drinking water exposure model. The first experiment used young (30 day old) female Swiss mice (n=16) that were exposed to 20 mM IDPN for 7 weeks. A second experiment compared 2-6-month-old male 129S1 (n=15), female 129S1 (n=12), and male Swiss mice (n=12). Groups of mice of these strains and sexes were exposed to 20, 30, or 40 mM of IDPN in the drinking water (n=4-6/group) for 4 (129S1) or 6 (Swiss) weeks. The third and fourth preliminary experiments included 4 groups of 4-6 adult female and 4 groups of 8 adult male 129S1 mice exposed to 0 (control), 25, 30, or 35 mM of IDPN for 5 or 8 weeks.

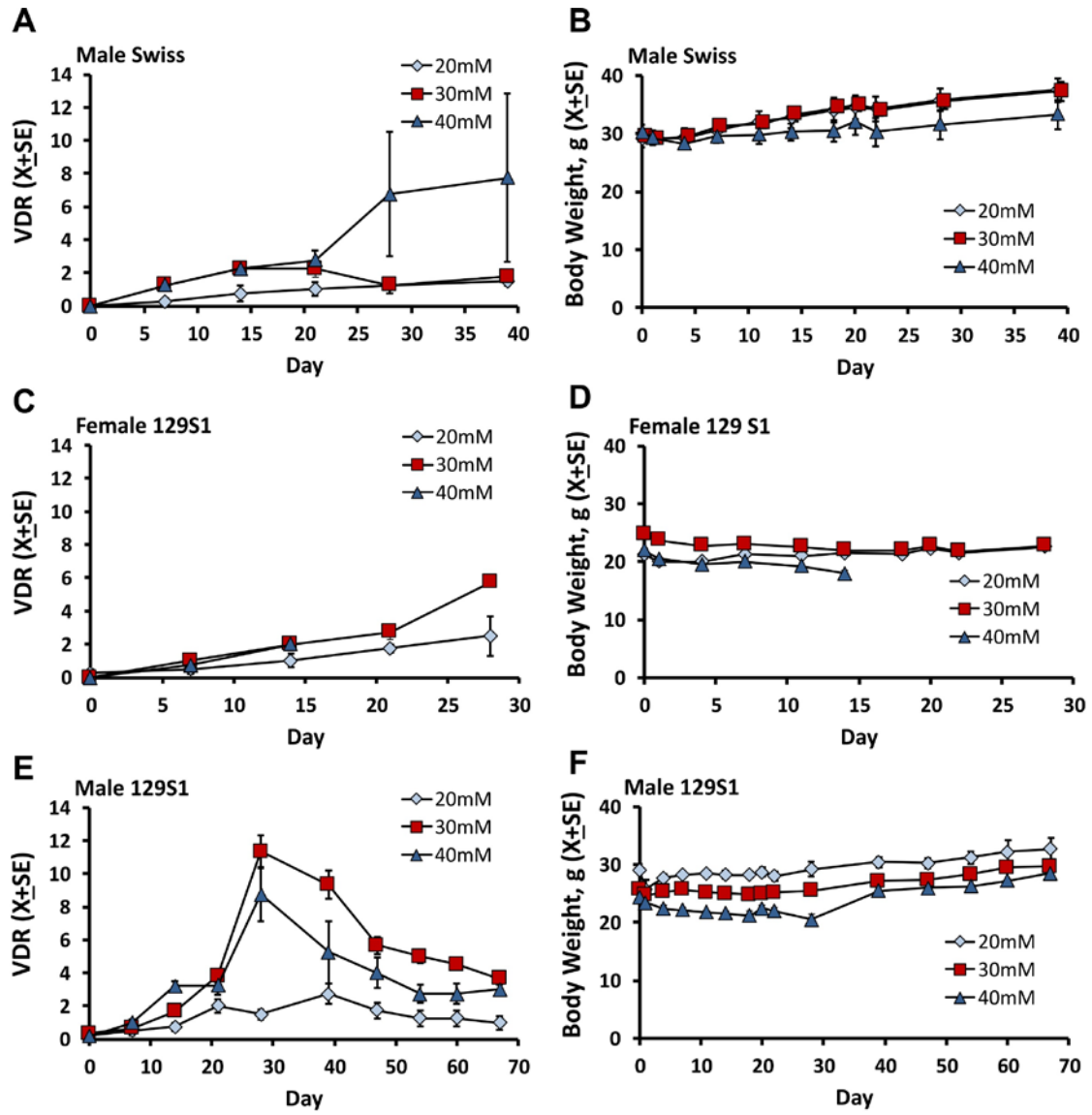
#### **Legends for supplementary figures**

Figure S1. Effects of IDPN (20, 30 or 40 mM in the drinking water) on vestibular function and body weight of mice. (A and B) Male Swiss mice (n=4/group) were exposed for 39 days. One animal in the high dose group displayed a large loss of vestibular function, but the other three in this group and those exposed to lower concentrations showed no effect. No large effects on body weight were recorded. (C and D) Female 129S1 mice (n=4/group) were exposed for 28 days. Three out of the four female 129S1 mice reached a 20 % loss of body weight by two weeks of exposure to 40 mM of IDPN, so the group was discontinued. Female 129S1 mice treated with lower concentrations showed only a weak loss of vestibular function at 4 weeks of treatment. (E and F) Male 129S1 mice (n=4-6/group) were exposed for 28 days and then allowed to recover for 40 days. In this experiment, one out of the five mice exposed to 40 mM reached a 20% loss of body weight by day 20, but none of the six animals exposed to 30 mM for 4 weeks did. These mice reached high VDRs that were largely reduced after exposure termination.

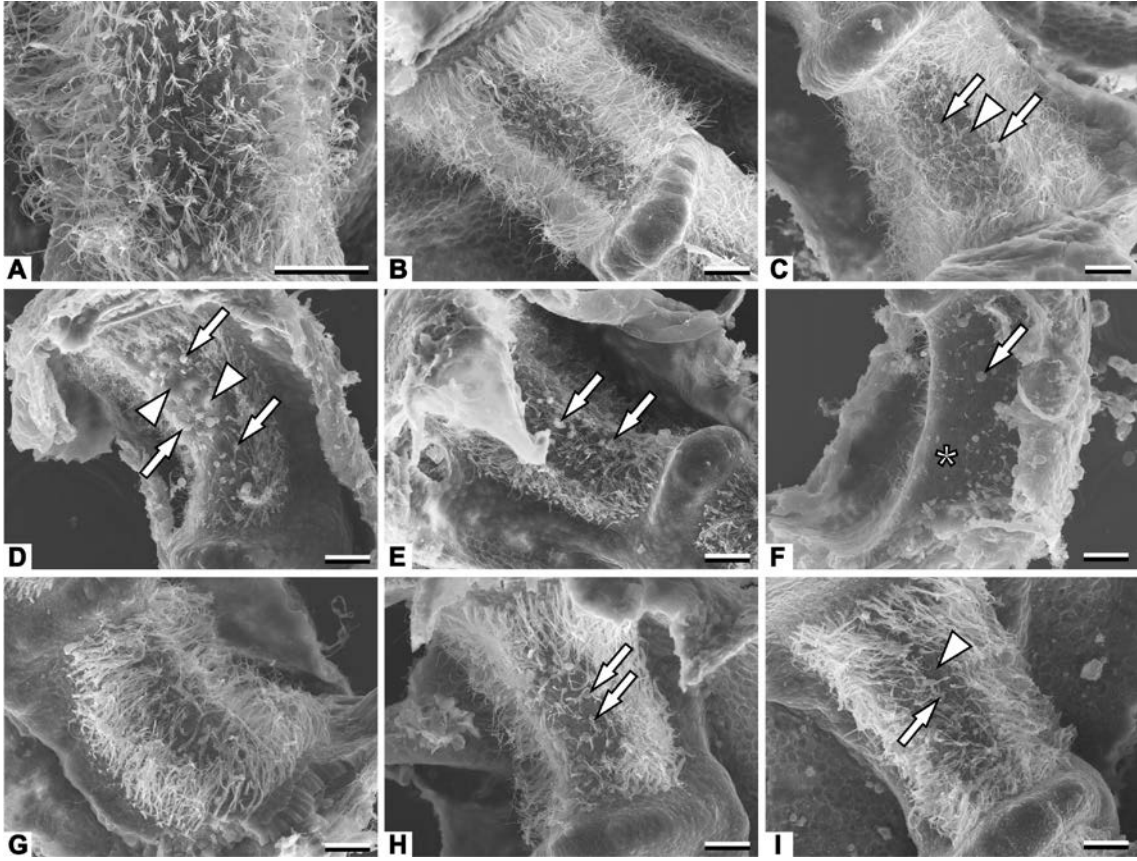
Three additional experiments were carried out and are not shown in Figure S1. (1) One group (n=16) young female Swiss mice were exposed to 20 mM of IDPN for 7 weeks. They showed no overt systemic toxicity and no effect on vestibular function. (2) Four groups of female 129S1 mice (n=4-6/group) were exposed to 0, 25, 30, or 35 mM of IDPN. The 25 mM concentration caused insufficient vestibular toxicity when administered for up to 8 weeks, while the 30 and 35 mM concentration caused excessive loss of body weight by 5 weeks of exposure. (3) Four groups of male 129S1 mice (n=8/group) were exposed to 0, 25, 30, or 35 mM of IDPN. The 25 mM concentration caused insufficient vestibular toxicity, while the 35 mM concentration

caused a vestibular effect similar to that of the 30 mM concentration, but with a larger effect on body weight.

Figure S2. Effects of IDPN (30 mM in the drinking water) on the vestibular cristae as assessed by SEM observation of the surface of the sensory epithelium. (A) Control mouse. A uniform distribution of stereociliary bundles indicate a normal density of HCs and supporting cells. (B-F) Cristae from mice exposed to IDPN for 8 weeks with diverse pathological stages. (B) Crista with a SEM Pathology Score of 0 from a mouse with a VDR of 5. (C) Crista with a SEM Pathology Score of 2 from a mouse with a VDR of 10; note the presence of coalescent stereociliary bundles (arrows) and spaces signaling absent HCs (arrowhead). (D and E) Two cristae from the same mouse showing diversity in the extent of the pathological alterations. Note extruding (arrows) and absent (arrowheads) HCs. This animal had a VDR of 10. Other animals in the study showed a similar pathology in the two cristae examined. (F) Crista of the worst-case mouse, displaying a VDR of 18 and a SEM Pathology Score of 5, with extensive loss of cells (asterisk) and ongoing extrusion of HCs (arrow). (G-I) Cristae from mice exposed to IDPN for 8 weeks and studied after a washout period of 13 weeks. (G) Crista with a SEM Pathology Score of 0 from a mouse presenting a VDR of 6 at 8 weeks, and a VDR of 1 after washout. (H) Crista with a SEM Pathology Score of 2 from a mouse presenting a VDR of 8 at 8 weeks, and a VDR of 1 after washout. Note the pathological hair bundles (arrows). (I) Crista with a SEM Pathology Score of 2 from a mouse presenting a VDR of 15 at 8 weeks, and a VDR of 1 after washout. Note pathological (arrow) and absent (arrowhead) hair bundles.



Suppl Fig 1



Suppl Fig 2